ELSEVIER

Contents lists available at ScienceDirect

Geochimica et Cosmochimica Acta

journal homepage: www.elsevier.com/locate/gca





Trace elements in zircon record changing magmatic processes and the multi-stage build-up of Archean proto-continental crust

Nadja Drabon^{a,*}, Heather M. Kirkpatrick^a, Gary R. Byerly^b, Joseph L. Wooden^c

- ^a Department of Earth and Planetary Sciences, Harvard University, Cambridge, MA, USA
- ^b Department of Geology and Geophysics, Louisiana State University, Baton Rouge, Baton Rouge, LA, USA
- ^c Unaffiliated, 785 Nob Ridge, Marietta, GA, USA (formerly at USGS Menlo Park and Stanford University, Stanford, CA, USA)

ARTICLE INFO

Associate editor: Tsuvoshi Jizuka

Keywords:
Zircon geochemistry
Continent formation
Hadean
Archean
Plate tectonics
Barberton Greenstone Belt

ABSTRACT

Zircon trace element geochemistry has become an increasingly popular tool to track crustal evolution through time. This has been especially important in early-Earth settings where most of the crust has been lost, but in some fortuitous instances detrital zircons derived from that lost crust have been preserved in younger sediments. To study the formation and geochemical evolution of continental crust from the Hadean to the Paleoarchean, the 3.6 to 3.2 Ga Barberton Greenstone Belt in southern Africa is an excellent target due to its outstanding preservation and presence of detrital zircons that span almost a billion years. Here, we use trace elements, in combination with hafnium and oxygen isotopes, of 3.65 to 3.22 Ga detrital and tuffaceous zircons of the Moodies and Fig Tree groups and compare their geochemistry to previously studied 4.2 to 3.3 Ga detrital zircons from the Green Sandstone Bed of the Onverwacht Group. The major detrital zircon age clusters in the former at 3.55 Ga, 3.46 Ga, and 3.26-3.23 Ga overlap with episodes of TTG emplacement and felsic volcanism in the Barberton area, suggesting a local provenance. In contrast, age clusters at 3.65 Ga and 3.29 Ga of the Moodies and Fig Tree groups as well as 4.2 to 3.3 Ga detrital zircons from the Green Sandstone Bed do not have known intrusive sources and were likely derived from outside the present-day Barberton belt. This indicates that more than half of the felsic igneous events in the detrital zircon record do not have a whole-rock representation that can be directly studied. The similar compositions and inferred crustal evolution histories recorded in zircons from the Fig Tree and Moodies groups, as well as from the Green Sandstone Bed, suggest that they were derived from connected terranes experiencing similar crustal processes diachronously. Together, they show three phases of felsic continent formation, reflecting different crustal processes: (1) long-lived protocrust formed in the Hadean from undepleted mantle sources. These zircons are vastly different from younger zircons and, hence, Barberton TTGs are not good analogues of Hadean crust formation. (2) At 3.8 Ga, onset of significant crustal growth though cyclic juvenile additions and hydrous melting, possibly within a volcanic plateau setting but an arc-like setting cannot be excluded based on this data. (3) Between 3.4 and 3.3 Ga, felsic crust is generated through a previously unrecognized episode of crustal growth by shallow melting of mafic, mantle-derived sources. This is immediately followed by the onset of crustal thickening through the transport of surface-altered, hydrated materials to deep crustal levels. Since there is geological evidence for extension and shortening at that time this may reflect the onset of horizontal movement. Whether this last geodynamic setting reflects modern-style plate tectonics or not, continent formation and the onset of plate tectonics in the Barberton area occurred through complex multi-stage processes spanning almost a billion years, most of which is only accessible through the detrital zircon record.

1. Introduction

The geochemical and tectonic evolution of Earth's continents remains a field of ongoing debate as crustal (and lithospheric) conditions were likely different from modern conditions during the early Earth, but

the effect of these differences is poorly understood. The timing of the onset of plate tectonics is controversially debated, whether it occurred as early as the Hadean (Hopkins et al., 2008; Harrison et al., 2017) or as late as the Neoproterozoic (Stern, 2005), and perhaps including several transitional stages over hundreds of millions to billions of years

E-mail address: ndrabon@fas.harvard.edu (N. Drabon).

^{*} Corresponding author.

(Cawood et al., 2022). Yet, the answer to this question is of importance to understanding Earth's habitability. Plate tectonics would have been a major driver in linking solid Earth with surface liquid and gaseous reservoirs, causing the emergence of crust above sea level, and thus initiating silicate weathering to stabilize Earth's climate and the release of nutrients into the oceans.

To address the evolution of tectonic processes, zircon has gained increasing popularity. The importance of zircon becomes especially pertinent when studying the early Earth, where ~95% of Archean crust has been lost (Goodwin, 1996) and almost no known rock exists for the Hadean Eon. For these time intervals, detrital zircons derived from the erosion of crust that has long been obliterated or is now deeply buried can provide insight into conditions and processes of these inaccessible terranes. While Hf and O isotope systematics have been applied to zircon for a long time, recent advances in understanding zircon trace and rare earth elements (TREE) (Grimes et al., 2015) have allowed for more complex evaluations of early crustal histories (Drabon et al., 2021, 2022; Carley et al., 2022; Laurent et al., 2022). They offer important clues into the formation and stabilization of ancient proto-continental crust during the Hadean to Archean.

The interpretation of zircon isotope and TREE chemistry is complex, as many different factors can affect zircon compositions, including zircon crystallization temperature, pressure, co-existing mineral assemblage, and magma source (Grimes et al., 2007, 2015; Claiborne et al., 2010). Interpreting Archean to Hadean zircons carries additional uncertainties because the higher heat flux from the mantle may have affected crustal conditions and tectonic processes. Most previous zircon TREE studies focused on Phanerozoic zircon suites. Yet, their results may not be directly applicable to Archean and Hadean zircon suites. However, the more general petrologic/magmatic conditions (shallow vs deep crustal melting, dry vs fluid-assisted melting, common fractionation patterns for mafic and felsic melts), as opposed to specific tectonic settings associated with the Grimes model, are applicable across time. Archean TTGs are generally thought to have formed from melting of a hydrated mafic rock at variable depth (Martin, 1986; Clemens et al., 2006; Moyen et al., 2006, 2007). The proposed environments may have ranged from uniformitarian plate tectonic environments (de Wit et al., 1987a,b, 2011; de Wit, 1991; de Ronde and de Wit, 1994; Lowe, 1994; de Ronde and Kamo, 2000; Kleinhanns et al., 2003; Moyen et al., 2006; Stevens and Moyen, 2007; Schoene et al., 2008; Kisters et al., 2010; Schoene and Bowring, 2010; Furnes et al., 2011, 2012, 2013; Laurie and Stevens, 2012; Nagel et al., 2012; Jagoutz et al., 2013; Arndt, 2023) to non-uniformitarian environments such as delamination melting (Bédard et al., 2013; Johnson et al., 2017; Bédard, 2018) and/or patrial convective overturn (Van Kranendonk, 2011, 2021; Van Kranendonk et al., 2014) within an oceanic plateau setting. It is therefore important to study the compositions of Archean zircons from well-studied exposed locations, which may have formed under non-uniformitarian conditions, and may more favorably compare to Archean and Hadean detrital or xenocrystic zircons with no known source.

The 3.6 to 3.2 Ga Barberton Granite-Greenstone Terrain (BGGT), South Africa and Eswatini, is uniquely qualified as a target for the study of Archean protocontinent formation due to its outstanding preservation, because the compositions of its intermediate to felsic igneous rocks are well known (Moyen et al., 2007, 2019; Moyen, 2011; Moyen and Martin, 2012; Laurent et al., 2022), and as it contains zircons that range in age from 4.15 to 3.22 Ga, spanning almost a billion years of Earth's history. Regional detrital zircon studies have shown that many of the detrital zircons were derived from known felsic igneous rocks in the vicinity (or from rocks of identical age and composition elsewhere) (Zeh et al., 2013; Drabon et al., 2017; Stutenbecker et al., 2019; Stoll et al., 2021; Drabon and Lowe, 2022; Heubeck et al., 2022), with several notable exceptions: The major ~3.29 Ga and minor ~3.65 Ga detrital zircon age clusters from sandstones of the 3.22 Ga Moodies and 3.28-3.23 Ga Fig Tree groups (Drabon et al., 2017, 2019a; Stoll et al., 2021; Drabon and Lowe, 2022), and the 4.2 to 3.2 Ga detrital zircons of the Green Sandstone Bed (GSB) in the Onverwacht Group (Byerly et al., 2018; Drabon et al., 2021, 2022) have no documented source rocks.

In this study, (1) we assess what the detrital zircon trace and isotope geochemistry of detrital and tuffaceous zircons from the Moodies and Fig Tree Groups tells us about the crustal evolution of the BGGT. We compare the results to interpretations of bulk rock analyses and geological relationships of known sources to anchor our interpretations; (2) We then investigate what the zircon geochemistry tells us about detritus derived from unknown crustal sources, including >3.8 Ga detrital zircons from the Green Sandstone Bed (GSB) previously published by Drabon et al., (2021,2022) to test whether they may have been derived from Archean-style TTGs; (3) Finally, we will put the evolution of the source terranes into a process-oriented context to ultimately assess the formation and geochemical evolution of Archean proto-continental crust in the Barberton area.

2. Geological background and samples

The 3.6 to 3.2 Ga Barberton Granite-Greenstone Terrane is located in the eastern Kaapvaal Craton. It is composed of three stratigraphic units: the Onverwacht, Fig Tree and Moodies Groups (Fig. 1A and B). Whereas the Onverwacht Group is dominated by mafic and ultramafic volcanic rocks punctuated by two episodes of felsic igneous activity, the Fig Tree and Moodies Groups represent the onset of orogeny and syndeformational deposition of siliciclastic and volcaniclastic rocks. The rocks are excellently preserved for Archean rocks, having mostly experienced lower-greenschist-facies metamorphism (Xie et al., 1997; Tice et al., 2004).

The BGGT experienced several episodes of felsic igneous activity that were sources to the zircons studied here. The Onverwacht Group, dating from 3.55 to \sim 3.26 Ga, experienced at least two significant periods of rhyolitic and dacitic volcanic activity associated with the intrusion of tonalite-trondhjemite-granodiorite (TTG) plutonic rocks. These include the 3.51 Ga Steynsdorp gneiss and felsic volcanic rocks of the 3.55 Ga Theespruit and Sandspruit formations (Armstrong et al., 1990; Byerly et al., 1996; Kröner et al., 2016; Roerdink et al., 2016). At ~3.45 Ga, the emplacement of the Stolzburg and Theespruit plutons took place penecontemporaneously to the deposition of felsic volcanic rocks of the H6 member of the Hooggenoeg Formation (Kröner and Todt, 1988; Armstrong et al., 1990; Kröner et al., 1991; Byerly et al., 1996). The presence of thin felsic tuffs suggests that further episodes of felsic volcanic activity may have occurred predominantly outside the present-day BGGTat 3472 Ma in the Hooggenoeg Formation, at 3280 \pm 9 Ma and 3287 \pm 3 Ma in the Mendon Formation (Decker et al., 2015), and at ~3280 Ma in the basal Fig Tree Group (Drabon et al., 2019a). Younger intrusive rocks include the 3.28-3.22 Ga Badplaas complex (Kisters et al., 2010), and the coeval 3.23 Ga Kaap Valley (Robb et al., 1986; Kamo and Davis, 1994; de Ronde and Kamo, 2000) and Nelshoogte plutons (Schoene et al., 2008; Matsumura, 2014).

Samples analyzed for this study were previously dated by Drabon et al., (2017,2019a) and Drabon and Lowe (2022) (Fig. 1C). Seven sandstone samples were taken from the Fig Tree Group (SAF-600-3, BARB5-DZ2, BARB5-DZ4, NAD-89, SAF-663-14, BSoI-S3-1, SSF-1) and two from the Moodies Group (SAF-663-13, NAD-130). Sediments of the Fig Tree Group were mostly derived from local uplifts of supracrustal rocks of the BGGT (Lowe and Nocita, 1999; Drabon et al., 2019a, 2019b; Drabon and Lowe, 2022). During Moodies time, erosion reached into deeper crustal levels because conglomerates also include granophyre clasts from the upper levels of shallow plutons or as erupted magma clasts (Eriksson, 1980; Reimer et al., 1985; Heubeck and Lowe, 1999; Sanchez-Garrido et al., 2011; Agangi et al., 2018). A major provenance region was likely the Stolzburg block (Zeh et al., 2013). The Ancient Gneiss Complex (AGC), an old terrane partially outcropping to the south of the present-day BGGT and in Eswatini (Fig. 1B), was apparently not exposed then (Heubeck et al., 2022). We also analyzed five volcanic and volcaniclastic samples of the BGGT sequence: SA-681-5 and SA-971-1

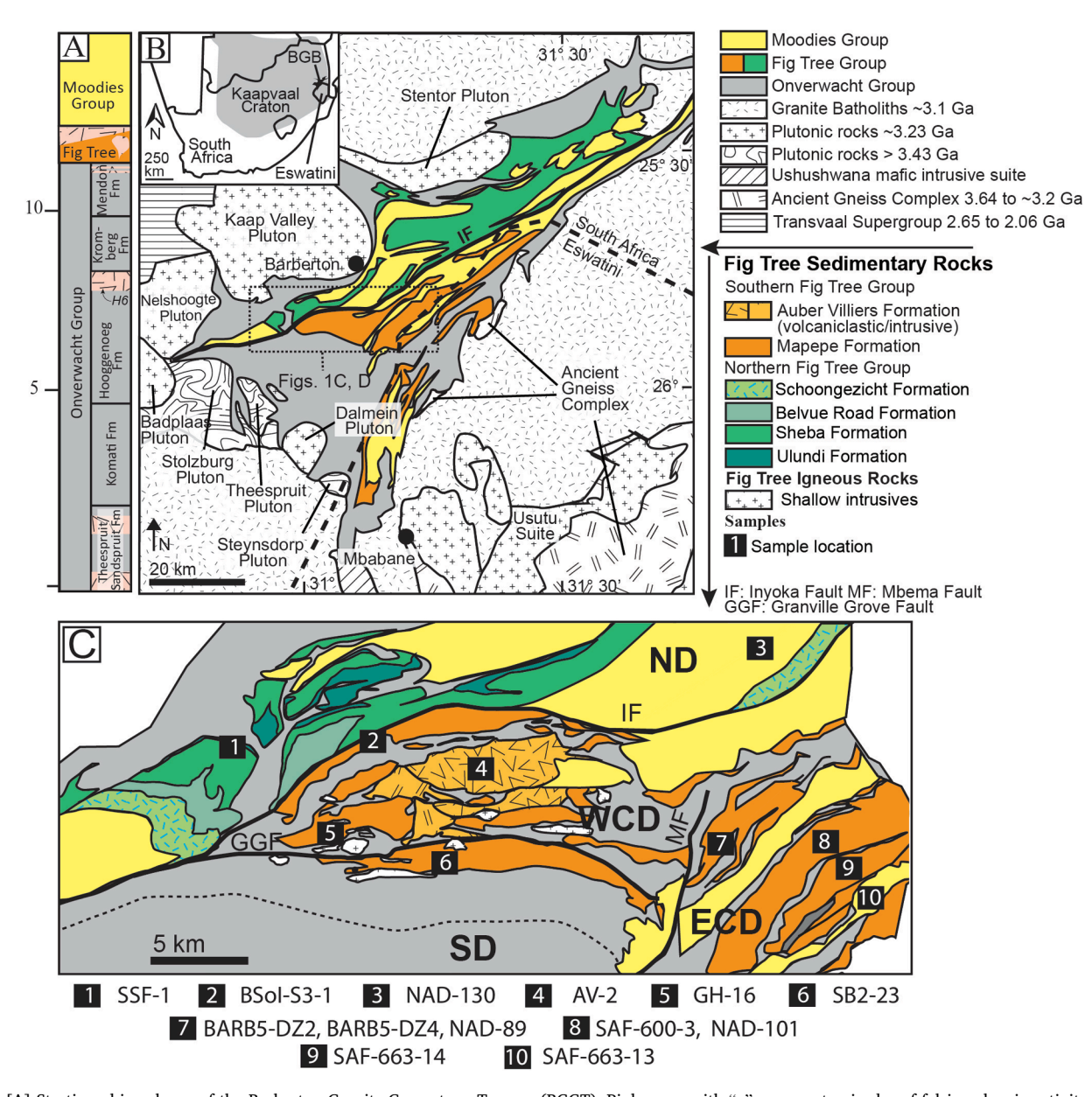


Fig. 1. [A] Stratigraphic column of the Barberton Granite-Greenstone Terrane (BGGT). Pink areas with "v" represent episodes of felsic volcanic activity that may have sourced the sediments to the Fig Tree and Moodies groups. [B] Geological map of the Barberton Greenstone Belt with possible plutonic sources within the BGGT and in the vicinity. [C] Geological map of the central BGGT (Lowe et al., 2012) with sample names and locations. GPS locations can be found in Drabon et al., (2017,2022).

from a dacitic tuff from the \sim 3.46 Ga H6 unit of the Hooggenoeg Formation of the Onverwacht Group, SB2-23 and NAD-101 from a 3.28 Ga rhyolitic tuff from the Loenen Member of the Fig Tree Group, and AV-2, a 3.23 Ga dacitic volcaniclastic rock from the Auber Villiers Formation of the Fig Tree Group.

Together, samples show age clusters at ~3.55 Ga, ~3.46 Ga, ~3.29 Ga, and 3.26–3.23 Ga (Figs. 2 and S1) and a single 3.65 Ga zircon. Previous work suggests the 3.55 to 3.51 Ga ages correspond to possible sources from the Theespruit Formation felsic volcanic rocks and comagmatic Steynsdorp tonalitic gneisses, and the ~3.46 Ga cluster from the felsic volcanic rocks of the H6 member of the Hooggenoeg Formation and its co-magmatic 3.46 Ga TTG suite (Drabon et al., 2017, 2019a; Drabon and Lowe, 2022; Heubeck et al., 2022). Zircon grains with an age of ~3.29 Ga form a major cluster, but only relatively minor felsic rocks of that age are present within the BGGT: thin 3.30 – 3.28 Ga tuffs in the upper Mendon Formation (Byerly et al., 1996; Decker et al., 2015) and 3.28 Ga reworked tuffs in the lower Mapepe Formation

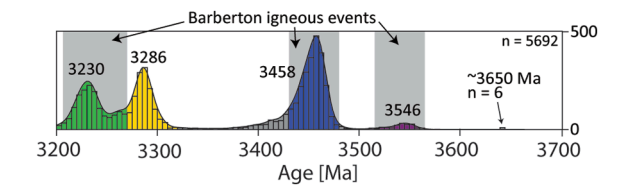


Fig. 2. Detrital and tuffaceous zircon samples from the BGGT (Drabon et al., 2017, 2021; Heubeck et al., 2022; Stoll et al., 2021; Stutenbecker et al., 2019). See Fig. S1 for individual detrital zircon sample probability density plots studied here.

(Drabon et al., 2019a). This may suggest the presence of a much larger source outside the preserved BGGT. The youngest detrital zircons between 3.26 and 3.22 Ga correspond to felsic volcanic rocks of the upper Fig Tree Group that are widespread across the BGGT and potentially

exposed upper segments of the Kaap Valley Tonalite, Nelshoogte pluton, Badplaas pluton, and Usutu magmatic suite or their extrusive equivalents (Fig. 1B).

3. Methods

3.1. Data acquisition

We obtained zircon TREE, Hf and O isotope data following the protocol described in Drabon et al. (2022). Zircon trace element analyses were conducted on the SHRIMP-RG ion microprobe in the co-operated Stanford and U. S. Geological Survey SUMAC facility at Stanford University, using techniques described by Grimes et al. (2015). Lu-Hf isotopic analyses were conducted at the Arizona LaserChron Laboratory, following methods previously described (Gehrels and Pecha, 2014; Ibanez-Mejia et al., 2014). Oxygen isotopic analyses were conducted using a Cameca 1280-HR SIMS at the Helmholtz Zentrum Potsdam. Where zircon grains were large enough, we tried to couple geochemical criteria within the same zircons, but that was only possible in a subset of zircons due to their small size. For complete information on analytical methods and our data compilation, we refer the reader to the supplementary material and the data repository at https://doi.org/10.17632/zmj566r6m4.1.

3.2. Filtering of Hf, O, and TREE data

Isotopic and chemical measurements on zircon can be biased by analyses of radiation-damaged areas, fractures, or inclusions. During analyses we avoided sites with visible impurities. The targets were subsequently examined under transmitted light microscopy to identify any analysis locations situated on subsurface cracks or inclusions. All data where the analytical pits revealed such fractures or inclusions were excluded from our study. Additionally, CL imaging of the zircons was used to filter out grains with homogeneous or patchy zoning and to ensure the analyses were conducted within the same crystallographic domain as the U-Pb dating (Hoskin and Black, 2002; Cavosie et al., 2005). Representative CL images were published by Drabon et al. (2019). For δ^{18} O analyses, zircons with low 16 O counts per second were discarded. For TREE analyses, we used conservative geochemical filters to exclude any data that signified enrichments of non-constituent cations, as these may indicate contamination or alteration related to metamictization (Grimes et al., 2015). Ca (>50 ppm) and P (>1000 pm) serve as screens for apatite inclusions, and Al (>100 ppm) as a screen for glass or feldspar inclusions, or altered (i.e., metamict) domains. Finally, we applied the Light Rare Earth Element Index (Bell et al., 2015) and excluded zircons with values < 20. Means and ranges for each age cluster are summarized in Table 1.

3.3. Zircon trace elements as recorders of magmatic environments and melting depth

We use zircon trace and rare earth element (TREE) patterns to evaluate the geochemical evolution of the zircon-sourcing magmas based on magmatic origin and the melting depth of the zircons.

Trace element ratios including those involving U, Th, Nb, Sc, Ce, and Yb provide a compositional distinction among zircons from different modern tectono-magmatic settings (Grimes et al., 2015). The Sc/Yb and U/Nb ratios in zircons have proven to be particularly useful in distinguishing zircons from melts that formed in undepleted mantle settings (today's ocean island settings, plumes), depleted mantle settings

Table 1Means, minimums, and maximums for each age cluster. Only one zircon was analyzed for the 3.65 Ga age cluster. Errors are 1sig.

		3.65 Ga	3.55 Ga	3.46 Ga	3.29 Ga		
					Group 1	Group 2	<3.28 Ga
Sc/Yb	mean	0.51 ± 0.11	0.10 ± 0.07	0.15 ± 0.08	0.15 ± 0.11	0.03 ± 0.01	0.25 ± 0.19
	min	N/A	0.05	0.03	0.08	0.008	0.06
	max	N/A	0.33	0.34	0.7	0.06	0.6
U/Nb	mean	72 ± 12	42 ± 28	55 ± 31	57 ± 30	45 ± 114	29 ± 14
	min	N/A	15	16	21	11	5
	max	N/A	127	135	167	67	73
Dy/Yb	mean	0.28 ± 0.07	0.32 ± 0.07	0.27 ± 0.08	0.31 ± 0.07	0.34 ± 0.05	0.38 ± 0.14
	min	N/A	0.19	0.1	0.14	0.24	0.17
	max	N/A	0.46	0.46	0.5	0.43	0.68
Nb/Ta	mean	1.2 ± 0.3	1.1 ± 0.7	1.8 ± 1.7	2.5 ± 2.2	4.0 ± 2.2	1.2 ± 0.6
	min	N/A	0.4	0.3	0.4	0.06	0.05
	max	N/A	2.5	9.9	7.8	8.6	2.1
Eu/Eu*	mean	0.24	0.23 ± 0.8	0.36 ± 0.13	0.29 ± 0.12	0.17 ± 0.1	0.43 ± 0.17
	min	N/A	0.09	0.18	0.03	0.06	0.1
	max	N/A	0.36	0.8	0.5	0.49	0.88
Ti	mean	5.0 ± 1.1	9.2 ± 5.7	6.6 ± 4.3	8.2 ± 2.9	4.8 ± 1.8	7.9 ± 4.6
	min	N/A	4.1	0.3	0.2	1.9	3.2
	max	N/A	35.1	17.9	13.3	12.3	18.5
$\delta^{18}O$	mean	N/A	5.5 ± 0.3	5.6 ± 0.3	5.9 ± 0.4	5.65 ± 0.3	6.6 ± 0.7
	min	N/A	5	4.6	5.3	4.7	5.1
	max	N/A	5.9	6.7	7.1	6.1	8.3
$\epsilon_{ m Hft}$	mean	N/A	0.8 ± 1.7	0.8 ± 1.8	0.1 ± 1.8	1.6 ± 2.5	-0.1 ± 2.1
	min	N/A	-0.9	-3	-3.7	-2	-5
	max	N/A	5.5	6.4	3.7	8.2	5.4

(today's MOR and oceanic arcs) and subduction zones where fluidassisted melting is a major feature (Grimes et al., 2015). Sc/Yb values are relatively elevated for zircons in fluid-rich arc environments (roughly > 0.1). In contrast, mafic magmas from the depleted or relatively undepleted mantle require extensive fractionation before zircon can crystallize, resulting in low Sc and low Sc/Yb values (Grimes et al., 2015). The relationship between U and Nb in magmatic systems is affected by factors such as influenced by variations in mantle source composition (depleted vs undepleted mantle source), depth of melting, metamorphic dehydration of oceanic crust (Pearce, 1982; Baier et al., 2008), and crustal assimilation (Grimes et al., 2015). In U/Yb versus Nb/ Yb diagrams, analyses of mantle zircons have delineated an observationally constrained mantle trend, with the upper limit approximately correlating to a U/Nb ratio of 20. In contrast, zircons formed in subduction zones tend towards higher U/Nb values due to a relative depletion in Nb and enrichment of U. While Grimes et al. (2015) found that these proxies can be used to identify zircons formed in modern arc settings, it is clear that other tectonic processes may impart a similar TREE signature because the specific magmatic conditions or processes that produce melts may be similar (presence of water, melting depth, etc). Therefore, we will term signatures of, e.g., Nb depletion and Sc enrichment, as documented by zircons derived from Phanerozoic subduction zones, as "fluid-assisted melting", "hydrous" or "arc-like" melting signatures in this manuscript, without intending any specific geodynamic interpretation.

Depth indicators in zircon are related to the presence or absence of certain pressure-dependent mineral suites during melt fractionation or in the residuum. Important minerals included plagioclase (Eu/Eu*), rutile (Nb/Ta), and garnet (Y, Dy/Yb).

Plagioclase is stable at relatively shallow depths and unstable at high pressure environments (Green, 1982). Plagioclase incorporates Sr^{2+} , which is geochemically similar to Eu^{2+} . Residual plagioclase in the source during melting or fractionation of plagioclase during fractional crystallization will draw down the $\mathrm{Eu/Eu}^*$ ($\mathrm{Eu_N/(Sm_N \times Gd_N)^{0.5}}$) of a melt, and hence the $\mathrm{Eu/Eu}^*$ value of the subsequently crystallizing zircon. $\mathrm{Eu/Eu}^*$ is also affected by the oxygen fugacity of the melt (Hoskin and Schaltegger, 2003; Trail et al., 2012). In general, $\mathrm{Eu/Eu^*}$ values in zircons from arc suites can vary a lot depending on gross melt evolution, but many have $\mathrm{Eu/Eu^*}$ in the 0.4–0.7 range; Iceland, ocean rift and Hawaiian zircons typically have $\mathrm{Eu/Eu^*}$ 0.2–0.4 (Grimes et al., 2015) in large part because of extensive plagioclase fractionation before zircon saturation. As the crust thickens, the increased pressure during magmatic differentiation at greater depths enhances rutile, amphibole and/or garnet fractionation relative to plagioclase.

Nb/Ta values of a melt can provide information on the tectonic setting, source composition, mineral assemblage, and pressure. Generally, primitive arc and basalt magmas have high Nb/Ta while more mature arcs tend to have low Nb/Ta (Tang et al., 2019). The reason for the low Nb/Ta in arc is still debated. It may to some extent be controlled by the presence or absence of rutile in the crystallizing fraction or residue. While the pressure dependence of rutile saturation is heavily debated (Ryerson and Watson, 1987; Gaetani et al., 2008; Xiong et al., 2009), recent studies have found that rutile solubility is reduced at high pressures (Tang et al., 2019). This means that greater differentiation at higher pressures will result in a greater amount of rutile forming. Due to its high partition coefficients for Nb and Ta, rutile formation will impart a strong signal on [Nb/Ta]_{melt}. Elevated titanite-to-rutile ratios result in melts characterized by exceptionally high Nb/Ta (>60), whereas reduced titanite-to-rutile ratios lead to melts with significantly lower Nb/Ta (≤30) (John et al., 2011). When all Ti-phases are completely consumed during intense melting, the Nb/Ta drops to very low levels (<16). As the titanite-to-rutile ratio is influenced by pressure, the Nb/Ta of melts becomes dependent on the depth of melting (John et al., 2011). In addition to rutile, the presence of amphibole or biotite has also been theorized to explain why continental crust demonstrates a lower average Nb/Ta ratio relative to chondritic values, since both amphibole and

biotite preserve a D_{Nb}/D_{Ta} ratio exceeding 1 (Stepanov and Hermann, 2013; Li et al., 2017). In addition, both of these minerals are Ti sinks that have temperature-controlled stability with greater Ti content in higher temperature amphibole (Ernst and Liu, 1998), making it less favorable for rutile to form.

Garnet is commonly used to argue for high-pressure environments that formed at great depth, although some exceptions occur. Garnet shows high partition coefficients for HREE and Y, and its crystallization results in an increase of the Dy/Yb of the melt (Dy/Yb > 0.4 in zircon are typically associated with garnet, although the fractionation of/presence of amphibole in the residuum prior to zircon crystallization may lead to lower Dy/Yb values even when associated with garnet). Typically, garnet-bearing source rocks will also contain rutile. Collectively, melts generated at greater pressure should thus exhibit high Dy/Yb and Eu/Eu*, and low Y, Yb and Nb/Ta. On the other hand, a Dy/Yb range of 0.1 to 0.4 for zircon is common within many magmatic systems (Grimes et al., 2015) and Dy/Yb decreases during simple mineral fractionation and cooling. Values for zircon less than 0.2 are found in more fractionated samples or at zircon edges.

4. Results

The results of the geochemical and isotopic analyses are shown in Figs. 3-7 and in the online repository. For all plots, we color-coded the data based on the relevant age clusters recognized by previous studies: ~3.55 Ga, ~3.46 Ga, ~3.29 Ga, and <3.28 Ga (Zeh et al., 2013; Drabon et al., 2017; Stoll et al., 2021; Drabon and Lowe, 2022; Heubeck et al., 2022). The geochemical and isotopic signatures of detrital zircons from these age clusters largely overlap between zircons derived from the Fig Tree and Moodies Group sandstones, suggesting a similar provenance. Zircons from the 3.46 Ga, 3.29 Ga, and 3.26 Ga age clusters extracted from tuffs and reworked tuffs (Figs. 3-7) also overlap in composition with those from the Moodies and Fig Tree Groups, which may indicate a source-sink relationship. Many detrital zircons from individual age clusters show some amount of heterogeneity, which may hint at subpopulations from distinct sources, as is reasonable to expect since many of these felsic igneous episodes span several tens of millions of years. While we focus on broader trends here, future work on possible subpopulations tied to more precise ages will be necessary.

4.1. TREE indicators for tectono-magmatic settings

We studied trace element ratios including those involving U, Th, Nb, Sc, Ce, and Yb to evaluate the tectono-magmatic origin of the Barberton zircons. All age clusters show at least some influence of fluid-assisted melting (Figs. 3 and 4): the single 3.65 Ga zircon, ~30% of zircons of the 3.55 Ga, and $\sim\!80\%$ of the 3.45 Ga age zircons fall within the arc-like field for U/Nb and Sc/Yb. The 3.29 Ga zircon cluster shows the largest amount of heterogeneity in Sc/Yb. This variability broadly translates to other TREE proxies such as Nb/Ta and Eu/Eu* as well. We therefore use the Sc/Yb data to separate the zircons of the 3.29 Ga cluster into Group 1 (>0.07) and Group 2 (<0.07) (Fig. 3). While the origin of the compositional variability remains unclear, considering these zircons as distinct compositional varieties facilitates contrasting the diverse potential endmember processes or sources capable of generating the observed range of geochemical signatures. Sc/Yb values for Group 1 fall almost exclusively into the arc field. Group 2 zircons fall (by definition) entirely into the mantle field for Sc/Yb. Nb concentrations for Group 2 are typical for zircons from mafic mantle melts with U/Nb values at the high end of the mantle range, but appropriate for the high U concentrations which in part may be the result of strong melt fractionation (Fig. S2). Lastly, while most age clusters show a range in signature overlapping both with the mantle and arc fields, < 3.28 Ga zircons exclusively fall within the arc field for Sc/Yb and where arc-like and mantle fields overlap for U/Nb, largely driven by low U content.

It should be noted that in the U/Yb vs Nb/Yb diagram after Grimes

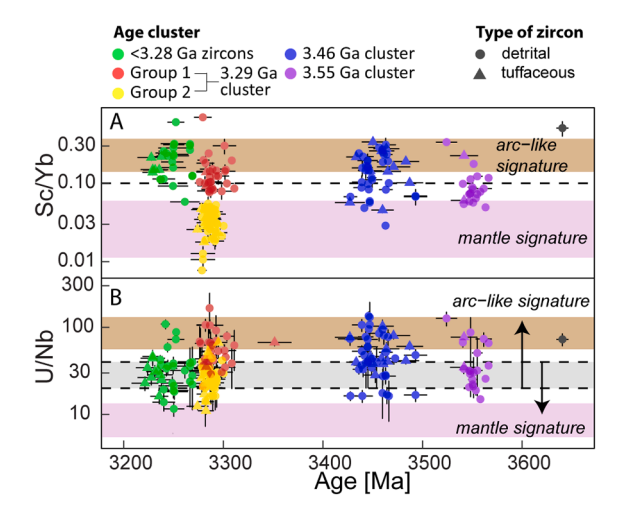


Fig. 3. [A] Sc/Yb and [B] U/Nb of detrital zircons from the Moodies and Fig Tree groups. Tectono-magmatic fields (first to third quartile) are from Grimes et al. (2015). Grimes zircon compilation was updated based on revision of the zircon reference material concentrations (Coble et al., 2018). The dashed lines reflect proposed bounding lines between different tectono-magmatic domains.

et al. (2015), the Barberton data plot in an intermediate position between the undepleted mantle and the arc fields (Fig. 4D). This may suggest that tectonic processes were different from modern-style plate tectonics or that the mantle composition was different (e.g., no clearly depleted and enriched reservoirs as seen today had formed yet). This mirrors observations from Archean whole rocks (Moyen and Laurent, 2018).

4.2. TREE indicators for melting depth

To understand variations in melting depth, we utilized Dy/Yb, Yb,

Eu/Eu*, and Nb/Ta ratios (Fig. 5). The 3.55 and 3.45 Ga age clusters show a similar range in Dy/Yb and Nb/Ta with only subtle differences (Figs. 5 and 6). For Dy/Yb, the values mostly range between 0.2 and 0.4 and show negative correlation with Hf/Ti (Figs. S3 and S4) as is common within many magmatic systems in the absence of garnet in the residuum or fractionating assemblage (Claiborne et al., 2010). Since most whole-rock data for 3.45 Ga TTGs show heavy REE depletion in agreement with garnet in the crystallizing fraction, it is likely that the zircons were derived from a rhyolitic/rhyodacitic volcanic source within the H6 member of the Onverwacht Group (Lowe, 1999; Diergaardt, 2013). These rocks may have originated through the differentiation of tonalitic

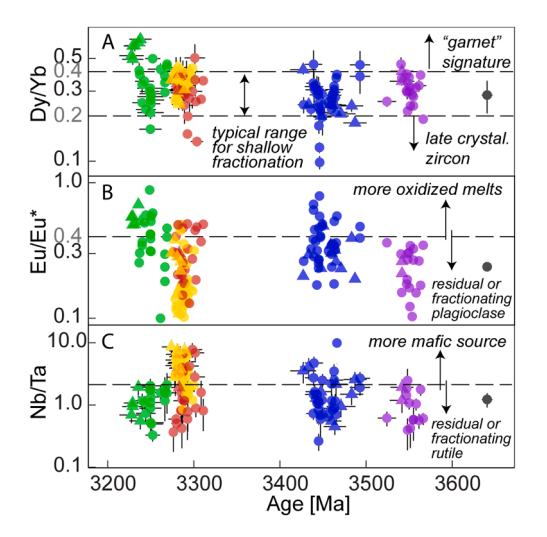


Fig. 5. Melting depth indicators [A] Dy/Yb, [B] Eu/Eu*, and [C] Nb/Ta vs age. Compositional and redox relationships are based on previous work (Trail et al., 2010; Grimes et al., 2015; Tang et al., 2021).

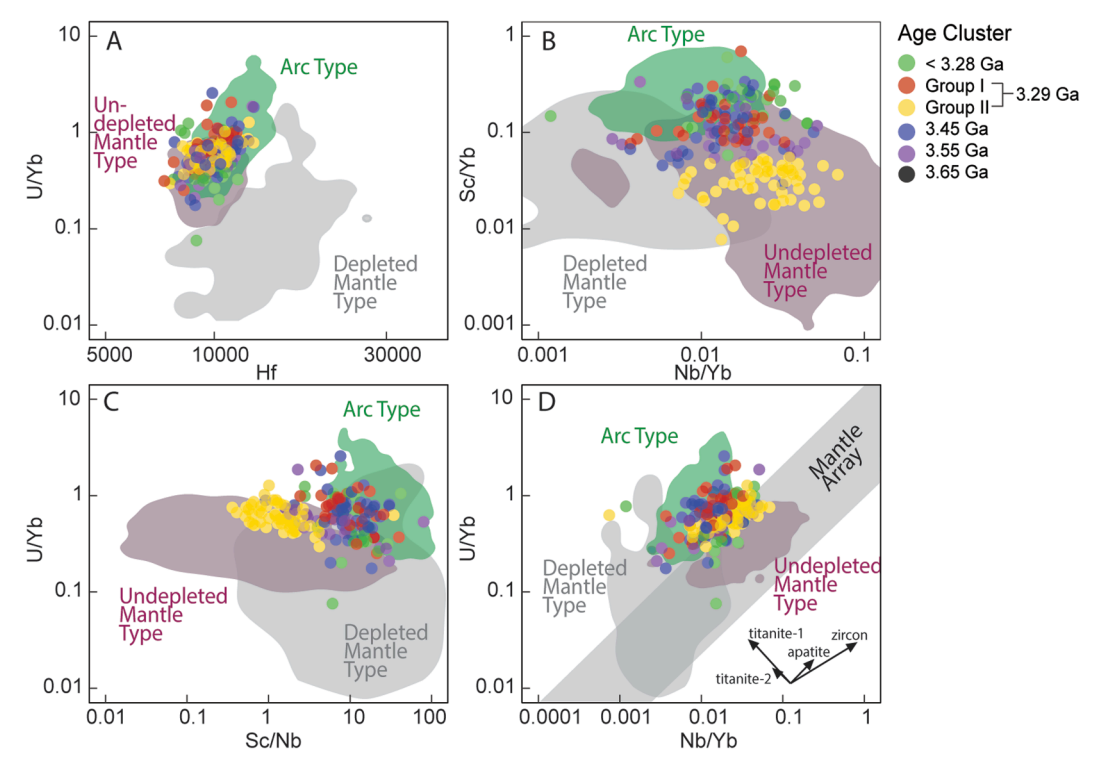


Fig. 4. Tectono-magmatic discrimination diagrams [A] U/Yb vs Hf, [B] Sc/Yb vs Nb/Yb, [C] U/Yb vs Sc/Nb, and [D] U/Yb vs Nb/Yb following Grimes et al. (2015). Grimes zircon compilation was updated based on revision of the zircon reference material concentrations (Coble et al., 2018). Plotted tectono-magmatic fields represent 90% of data.

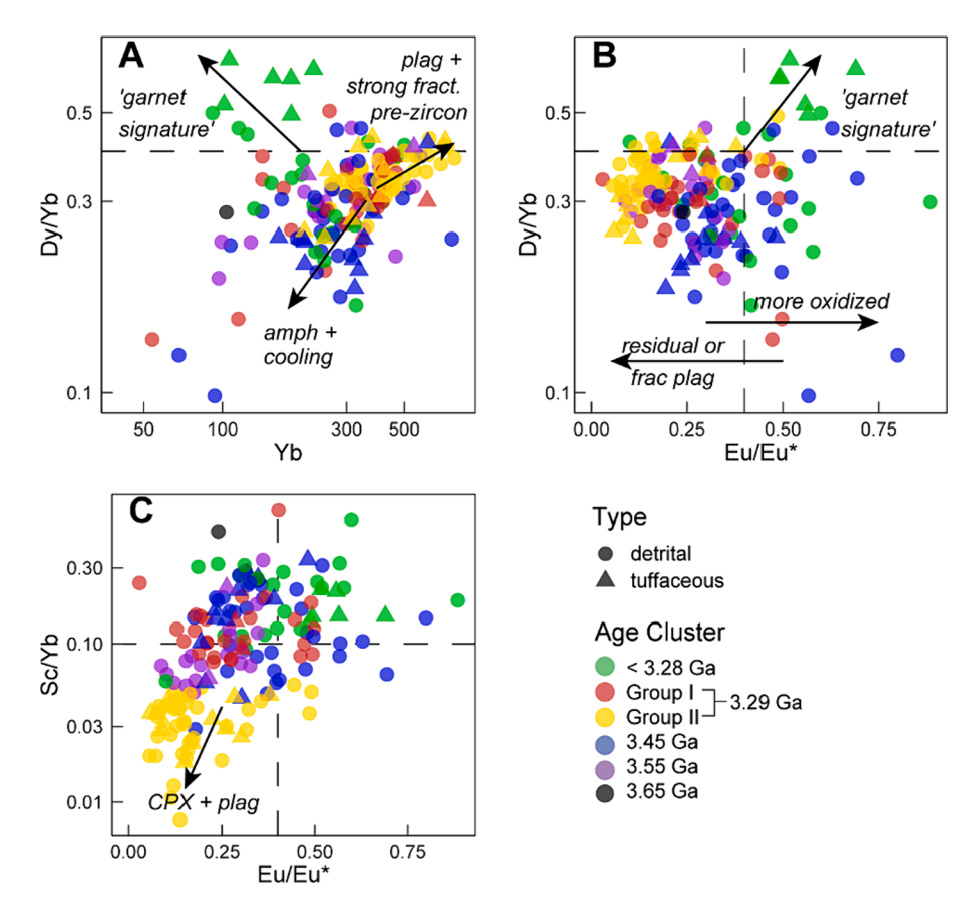


Fig. 6. Trace element diagrams. [A] Dy/Yb vs Yb, [B] Dy/Yb vs Eu/Eu*, and [C] Sc/Yb vs Eu/Eu*. Error bars are omitted for clarity. Diagrams are based on previous work (Grimes et al., 2015; Clemens-Knott et al., 2021).

magmas, with the residual liquids erupting as silicic volcanic rock (Laurent et al., 2022). It is also possible that presence of amphibole in the fractionating assemblage or residuum reduced the Dy/Yb ratio before zircon saturation was reached. Nb/Ta values are relatively low for both age clusters and are consistent with zircon crystallization from melts that had rutile in the fractionation or source mineral assemblage and thus indicate melts generated or fractionated at moderate to moderately high pressures. The most interesting difference between the two age clusters is their Eu/Eu* range, with the values for 3.55 Ga zircons lower than the 3.46 Ga zircons (Fig. 5). This possibly points at the suppression of plagioclase and hence a higher-pressure origin for the 3.45 Ga zircons compared to the 3.55 Ga zircons or may be a result of variable amounts of plagioclase in the residuum.

For the 3.29 Ga zircon cluster, Group 1 and 2 zircons compositions show indications for different melting depths and/or sources. Group 2 of the 3.29 Ga age cluster shows the highest Nb/Ta values of all age clusters while Group 1 shows lower values similar to the older age clusters (Fig. 5C). As discussed above, this could indicate a lower pressure origin, and/or a more mafic melt from a mantle source. A mafic composition that experienced strong fractionation prior to zircon saturation is supported by the lowest Eu/Eu* values of the entire zircon suite, high REE, high Y, and low Sc/Yb (Fig. 6). With the exception of Eu^{2+} , REEs are largely incompatible in plagioclase, hence plagioclase fractionation will produce or contribute to the production of REE-enriched magmas. This group also shows a correlation between Eu/Eu* and Sc/Yb (Fig. 6C). Mantle-related settings (MOR, OI) show low Sc values due to the extensive fractionation of ferromagnesian minerals. Here, the correlation between the two elements may relate to the coupled fractionation of plagioclase and clinopyroxene in a more mafic environment, likely at shallow depth. Group 1 of the 3.29 Ga age cluster shows higher Eu/Eu* values, does not show REE enrichment, and has lower but variable Nb/

Ta values compared to Group 2 (Fig. 5), possibly related to a higher-pressure crustal origin and/or mixing between mafic materials with preexisting crustal materials.

Zircons <3.28 Ga show variability with age in Dy/Yb, Eu/Eu*, and Nb/Ta (Fig. 5). Most notable are the high Dy/Yb (>0.4) combined with low Yb for 3.23 Ga zircons from the Auber Villiers Formation and a few isolated detrital 3.26 Ga zircons. This could indicate the presence of garnet in the crystallizing fraction or in the residuum. These results match whole rock analyses, which show a similar transition in Dy/Yb at 3.23 Ga (Wang et al., 2022b). In addition, these zircons have elevated Eu/Eu* values, which indicates a plagioclase-poor system and/or a more oxidized system. In fact, garnet fractionation may cause endogenic oxidation of Eu²⁺ (Tang et al., 2021). Overall, this pattern may reflect a deep melting origin of the youngest detrital BGGT zircons. The elemental composition, together with Sc and Nb, compares most favorably to modern arc environments (Grimes et al., 2015). Other zircons of the <3.28 Ga zircon suite show variable Dy/Yb, generally variable Eu/Eu*, and slightly decreasing Nb/Ta, possibly pointing towards melting at variable depth. This matches whole rock analyses, which show the start of more complex compositional variability and sources at variable depths for felsic igneous rocks < 3.28 Ga (Moyen et al., 2019).

4.3. Hf isotope systematics

The Lu-Hf isotope system tracks crust-mantle differentiation processes. ϵ_{Hft} values scatter \pm 5 units around CHUR (Fig. 7A, Table 1): The 3.55 and 3.45 Ga age clusters show a slightly superchondritic mean (0.8 \pm 1.7 and 0.8 \pm 1.8 ϵ_{Hft} units, respectively). The 3.29 Ga zircons' ϵ_{HfT} value is roughly chondritic for Group 1 (0.1 \pm 1.8 ϵ_{Hft} units) but superchondritic for Group 2 (1.6 \pm 2.5 ϵ_{Hft} units). Fig Tree-age zircon (<3.28 Ga zircon) show a slightly subchondritic value (–0.1 \pm 2.1). The

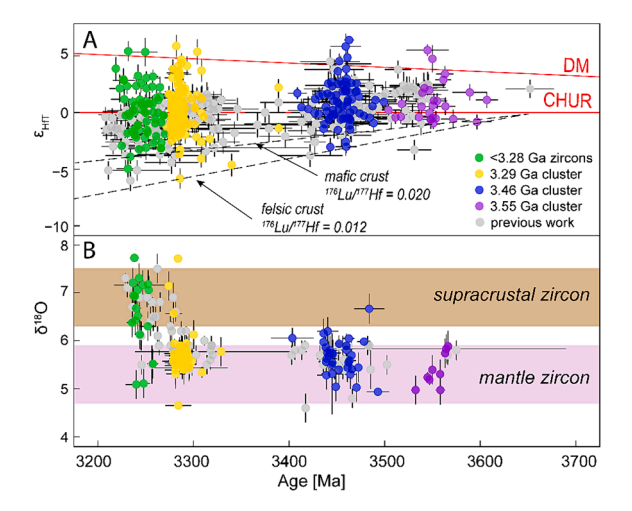


Fig. 7. Summary of isotope and geochemical analyses of zircons from the Fig Tree and Moodies groups. Gray dots show previous detrital zircon data (Zeh et al., 2013; H. Wang et al., 2022; X. Wang et al., 2022). See Fig. 8 for individual TREE Groups of the 3.29 Ga age cluster and Fig. S5 for the comparison to possible source lithologies.

Hf isotope measurement of a 3.65 Ga zircon burnt through the grain; a previously reported 3.65 Ga zircon from the Moodies Group has a value of $2.1\pm0.8\,\epsilon_{Hft}$ units (Fig. 7; Zeh et al., 2013). The isotope results agree with previous work on Moodies and Fig Tree detrital zircons (Zeh et al., 2013; Wang et al., 2022a) and matches those of granitoids from the BGGT and AGC (Fig. S5).

It is notable that the lowest ϵ_{Hft} values systematically decrease with age and are largely delineated by an inferred mantle extraction trend line from around 3.8 to 3.65 Ga (Fig. 7). If one assumes a single source, this means that the lowest ϵ_{Hft} values fall above a line of $^{176}\text{Lu}/^{177}\text{Hf}$ of 0.012, typical for felsic crust for all zircons; the vast majority fall above a line of $^{176}\text{Lu}/^{177}\text{Hf}=0.02$, typical for mafic crust. These crustal-evolution lines intersect with CHUR at 3.65 Ga. However, mantle extraction ages also depend on the evolution of the depleted mantle, which is poorly constrained (Petersson et al., 2020). If a depleted mantle had already formed, mantle extraction may have happened as early as 3.8 Ga. The highest ϵ_{Hft} values for every cluster are all superchondritic, reaching as high as 6 ϵ_{Hft} units. Overall, these results suggest that magmatism throughout the evolution of the BGGT continuously had two sources: reworking of older crust extracted from the mantle sometime between 3.8 and 3.65 Ga, and juvenile crustal additions.

4.4. O isotope systematics

Zircon's oxygen isotopes are a temperature-dependent proxy for fluid and solid interactions in the crust (Valley, 2003). The $\delta^{18}{\rm O}$ composition of the modern mantle has been well established and falls within a narrow range of $\delta^{18}{\rm O}$ of 5.3 \pm 0.6 % (2SD) (Valley et al., 1998, 2005; Cavosie et al., 2009). Elevated $\delta^{18}{\rm O}$ values in zircon (>6.3%) result from crystallization in magmas whose source materials (or major assimilants) have undergone low-temperature alteration prior to melting, while low $\delta^{18}{\rm O}$ values (<4.7%) result from high-temperature alteration by low $\delta^{18}{\rm O}$ surface water.

The O isotope data can be divided into two groups (Fig. 7B). Firstly, zircons older than 3.28 Ga show $\delta^{18}\text{O}$ values largely within the mantle field. Only a single 3.46 Ga zircon and three zircons of the 3.29 Ga Group 2 age cluster clearly plot within the supracrustal field. Secondly, there is an increase in $\delta^{18}\text{O}$ values starting at 3.28 Ga, reflecting the input of surface-altered materials into the melts. Fig Tree zircons show the highest values of all age clusters (6.6 \pm 0.7 %). These results are similar to previous work (Wang et al., 2022a; Wang et al., 2022b), albeit our data suggest that reworking of abundant surface-altered materials began

earlier (at 3.28 Ga) compared to the previously proposed ages of 3.26 and 3.23 Ga, respectively. This indicates that the shift from reworking of mantle material to surface-altered material coincides with the onset of Fig Tree deposition.

5. Discussion

5.1. Implications for the geological evolution of the BGGT

The geochemistry of Barberton zircons illuminates varied processes of felsic igneous crust generation. Since many geochemical signatures are non-unique, we use a synthesis of the isotopic and geochemical data compared to previous work on the geology, whole-rock geochemistry, and igneous petrology to infer the geological evolution of the BGGT.

The formation of the BGGT commenced prior to the formation of its oldest preserved rocks (3.55 Ga). Physical evidence for earlier crust formation comes from the presence of >3.55 Ga detrital zircons from the GSB (see Section 5.3), two 3.7 Ga xenocrysts in a 3.5 Ga granodiorite (Kröner et al., 1996), and rare 3.65 Ga detrital zircons from the Fig Tree and Moodies Groups (Zeh et al., 2013; Drabon et al., 2017; Heubeck et al., 2022). Additional indirect evidence comes from negative ε_{HfT} values of zircons from two tuffs from the Theespruit Formation (Kröner et al., 2016), a EHFT value significantly below CHUR for a single 3.55 Ga detrital zircon (Zeh et al., 2013) and ¹⁸²W isotope data of ultramafic to felsic rocks (Tusch et al., 2022). These low isotopic signatures may be related to the reworking of ancient GSB crust. Similarly, negative ε_{HfT} values in the AGC are also thought to be related to Hadean crust in the area (Hoffmann and Kröner, 2019). Yet, the bulk of 3.55 Ga zircons plot close to CHUR and yield mantle extraction ages ranging between ~3.8 Ga and 3.65 Ga (Fig. 7), close in age to the oldest detrital zircons within the Moodies and Fig Tree groups, making this the major episode of BGGT inception. While the analytical results of the single 3.65 Ga zircon need to be taken with caution and more analyses are certainly necessary, this initial melting may have been hydrous melting of juvenile crust (Figs. 3 and 4, Zeh et al., 2013). It appears that either pre-3.8 Ga materials consisted of isolated felsic crustal fragments that were rapidly reworked or that older crust was not involved in the younger magmatic episodes.

The oldest episodes of felsic crust production that are preserved within the BGGT whole-rock record occurred at \sim 3.55 Ga and 3.46 Ga. The 3.55 Ga zircons show evidence for second-stage melting of relatively juvenile rocks (largely chondritic ϵ_{HfT} , relatively low Sc/Yb and U/Nb) that were at least partially hydrated prior to melting (some elevated U/ Nb and Sc/Yb). Melting occurred in the plagioclase stability field. Mantle-like δ^{18} O values suggest that not much sedimentary rock was incorporated into the melts from which the zircons formed. Following this event of crustal growth, the 3.46 Ga felsic igneous episode represents the predominant reworking of pre-existing crust, with some juvenile additions. Its elevated U/Nb and Sc/Yb values suggest a more evolved composition with a stronger hydrous melting signature when compared to the 3.55 Ga crust. Based on lower ϵ_{HfT} values and the presence of 3.55 Ga xenocrysts, it is likely that some of the reworked crust included 3.55 Ga BGGT crust (Byerly et al., 1996). The presence of elevated ε_{HfT} values for both zircon clusters suggests continuous juvenile felsic additions. Previous work on the 3.51 Ga Steynsdorp gneiss showed that it formed at a shallower depth than the 3.45 Ga TTG suite, but both from an altered basaltic source (Moyen et al., 2019). This is consistent with our findings based on Eu/Eu*, Sc/Yb and U/Nb. While other explanations are also possible (Laurent et al., 2020), the reworking of hydrated crust remains a unifying feature.

The geochemistry of 3.29 Ga zircons reveals a previously unrecognized episode of felsic crustal growth. Group 2 zircons of this age cluster show a significant excursion into the mantle field for Sc/Yb. This signature is similar to modern intra-cratonic rift or plume settings (Grimes et al., 2015), which often yield low Ti values, such as the Silver Spring caldera (McDowell et al., 2014) or Salton Sea rifting (Lowenstern et al., 1997, 2006), or continental plumes such as Yellowstone (Stelten

et al., 2014). The somewhat elevated ε_{HfT} values of this age cluster compared to other clusters (Fig. 8A), suggest an increase in juvenile additions; mantle-like $\delta^{18}O$ values confirm a contribution of mantlederived materials. Their formation contemporaneous with komatiites of the 3.34 to 3.26 Ga Mendon Formation, which have been interpreted as forming in an extensional setting driven by a deep mantle plume (Lowe, 1994, 1999; Trower and Lowe, 2016), suggests a change in geodynamic setting consistent with our interpretation. This explanation is strengthened by the presence of bimodal (komatiitic and rhyolitic) volcanism at 3.29 Ga, a hallmark of extensional settings (Pedersen et al., 1998). However, we acknowledge that the tectonic settings of komatiitic volcanism are still debated and that more work is necessary on the tectonic setting of Mendon Formation komatiites. Moodies 3.29 Ga felsic conglomerate clasts and xenoliths (Kamo and Davis, 1994) should also be studied in more detail. In contrast, Group 1 zircons show a mostly hvdrous melting signature and relatively lower ϵ_{HfT} values (Fig. 9). The interpretation of these data in part depends on whether Group 1 and 2 of the 3.29 Ga age cluster reflect two separate sources or mixing of mantlederived magmas with pre-existing continental crust.

After 3.28 Ga, we find evidence for the most arc-like melting signatures, the recycling of surface-altered materials (this study; Wang et al., 2022a; Wang et al., 2022b) and, at least by 3.23 Ga, deeper crustal recycling. The Sc/Yb signature of zircons of this age group is most similar to that of zircons formed in modern arcs, and very few zircons plot within the mantle field (Fig. 3). The fact that the zircons do not fall exclusively in the arc field for U/Nb may be related to a more mafic source as postulated based on similarly aged whole rock analyses (Moyen et al., 2019), which could explain the lower U abundance. The positive shift in δ^{18} O of the zircons to supracrustal values shows that abundant material that had been altered in the presence of low-

temperature water was melted at depth. While the zircon Hf isotopes suggest mostly crustal reworking, there is also evidence for limited juvenile additions, as seen in isolated elevated ϵ_{HfT} values and the presence of a few zircons that show both: mantle-like Sc/Yb and δ^{18} O values. Melting depth was variable for <3.28 Ga zircons and includes the first occurrence of Dy/Yb > 0.4 and low Yb (Fig. 6A), which are both indicative of high-pressure melting in the presence of garnet. This interpretation matches previous explanations that these rocks formed from high-pressure, water-present partial melting of an eclogite facies metabasaltic source based on experimental work (Laurie and Stevens, 2012).

The crustal evolution of the BGGT apparently changed substantially at around \sim 3.3 Ga. One remarkable aspect of the older felsic episodes is the cyclicity of major events, with major felsic crust formation events occurring at ~100 Ma intervals at 3.65 Ga, 3.55 Ga, and 3.46 Ga. This apparent cyclicity suggests a repetitive nature to felsic crust generation. Elucidating the tectono-magmatic setting within which these zircons formed remains challenging due to the lack of modern analogues for possible non-uniformitarian tectonic settings. It is, however, clear that hydrous melting played a role throughout this time period to varying degrees, that there were significant mantle additions throughout, that newly generated magmas traversed through older felsic rocks as evidenced by the pervasive presence of xenocrysts (de Ronde et al., 1991; Kröner et al., 1991; Byerly et al., 1996; Decker et al., 2015; Drabon and Lowe, 2022), and that there is little evidence for deformation or the generation of topographic highs to generate siliciclastic rocks (Lowe, 1999). This has been used to argue for a complex interplay of magmatic accretion (Byerly et al., 1996; Moyen et al., 2019), delamination (Bédard et al., 2013) and/or cyclic partial convective overturn (Van Kranendonk, 2011; Van Kranendonk et al., 2015; Wiemer et al., 2018; Wang et al.,

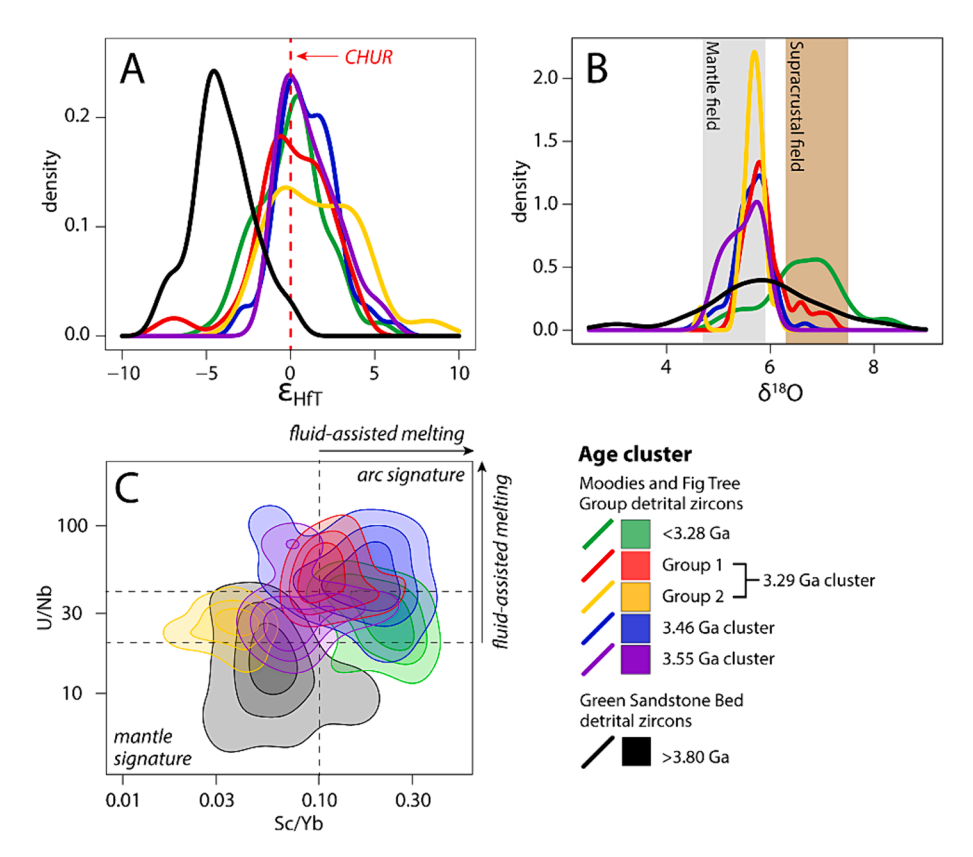


Fig. 8. Comparison of pre-3.8 Ga zircons of the GSB to detrital zircons of the Fig Tree and Moodies groups of the BGGT. [A] ϵ_{HfT} distribution, [B] δ^{18} O distribution, [C] U/Nb vs Sc/Yb (after Grimes et al., 2015). Data only plotted for grains that we have TREE data for. We did not correct for the radioactive decay of U within zircon in [C], because the abundance of U has decreased by the same proportion in all relevant reservoirs due to radioactive decay. Hence, not only zircon, but also the Hadean mantle, crust, and source magmas would have contained about twice as much U as today, all else equal. Thus, a comparison of uncorrected values allows a comparison at equal relative U abundance, irrespective of the time of crystallization.

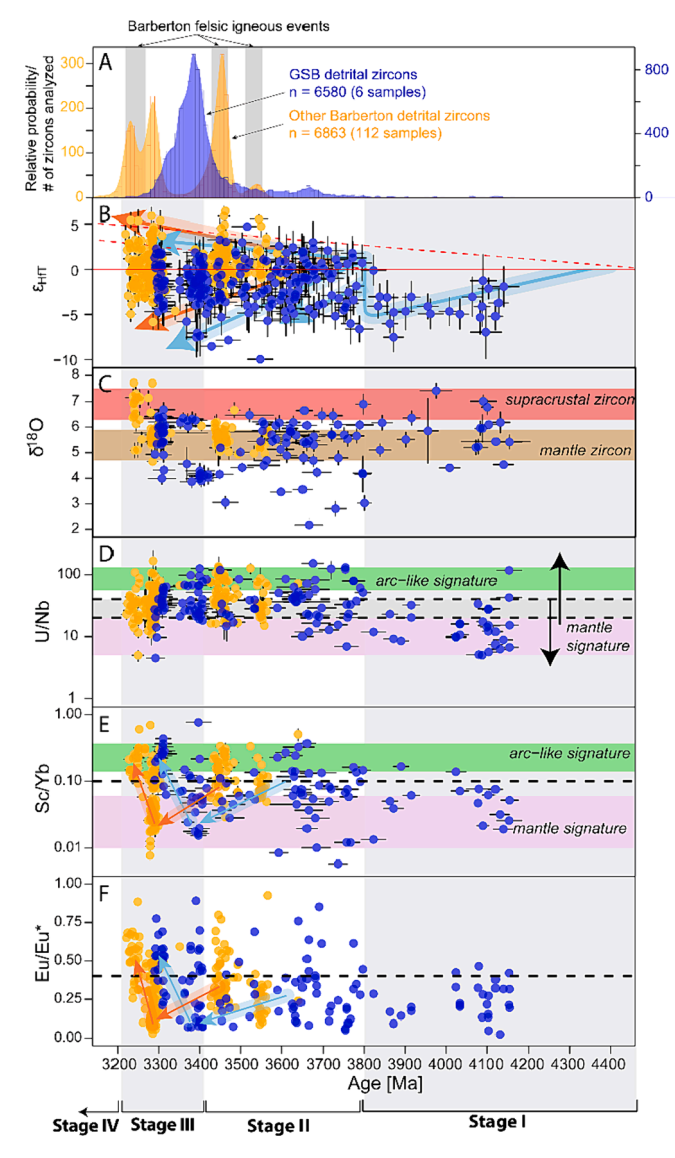


Fig. 9. Comparison of evolutions of the BGGT (this study) and the GSB zircons (Drabon et al., 2021, 2022). [A] Detrital zircon age distribution for the Green Sandstone Bed (Drabon et al., 2021; Byerly et al., 2018) compared to other data from the BGB (Zeh et al., 2013; Drabon et al., 2017, 2019, 2022; Stoll et al., 2021; Stutenbecker et al., 2019). Comparison of [B] $\epsilon_{\rm HfT}$, [C] δ^{18} O, [D] U/Nb, [E] Sc/Yb, and [F] Eu/Eu* values for the GSB (Drabon et al., 2022) to other data from the BGGT (this study).

2022a) in a magmatic plateau. Within a magmatic plateau, mafic crust that was altered and hydrated at the sea floor would provide the precursor crust that was reworked to form more felsic melts from which the zircons crystallized. However, a magmatic arc origin cannot be excluded based on the data presented here.

The cyclicity of crust generation ends around 3.3 Ga with a previously unrecognized episode of felsic crustal growth. Immediately following this event, volcanic activity occurred on a much shorter time scale, lacked cyclicity, and became compositionally more complex. In addition, this transition is associated with a major change in the stratigraphy of the BGGT; from a ~300 Myr period dominated by felsic and ultramafic igneous activity to the formation of thick siliciclastic, quartzrich sedimentary strata reflecting the generation of topography at the onset of the deposition of the Fig Tree Group. Different models have been proposed for this period, ranging from modern-style plate tectonics (de Wit et al., 1987b; De Wit, 1998; Moyen et al., 2006; Schoene et al., 2008; Kisters et al., 2010), squishy-lid tectonics (Moyen et al., 2019),

and partial convective overturn (Van Kranendonk, 2011, 2021; Van Kranendonk et al., 2015). While the zircon signatures are non-unique, we prefer a model in which at least some local horizontal plate motion occurred. This is because the shift in zircon geochemistry coincides with the onset of progressive accretion based on geological relations and geochronology of different structural belts within the Fig Tree Group (Drabon and Lowe, 2022). In addition, a recent structural and geochronological analysis by Heubeck et al., (2022) of the Malolotsha area confirmed earlier postulates for a minimum of 33 km of subhorizontal shortening towards the northwest, following Moodies deposition in this region. This supports earlier work that provides evidence for lateral motion (Lamb, 1984; Jackson et al., 1987; Lamb and Paris, 1988; Heubeck and Lowe, 1994; Dziggel and Kisters, 2019) complemented by evidence for some potential vertical mobility (Van Kranendonk, 2011, 2021; Schmitz and Heubeck, 2021), perhaps in a squishy-lid environment. This orogenic stage of the BGGT evolution had started by 3.28 Ga but peaked with the 3.23 Ga D2 deformation event (Lowe, 1999), when 3.23 Ga zircons record the strong deep crustal melting signature of hydrated material. Together, this may reflect the onset of crustal thickening through the transport of surface-altered, hydrated materials to deep crustal levels associated with the D2 event. Clearly, a change in the Barberton geology towards an orogenic stage is directly reflected in the zircon TREE and isotope geochemistry.

5.2. Are Archean TTGs potential analogues to Hadean source rocks?

Hadean zircons are the only record of the Earth's first 500 Ma of history. While these zircons reveal a plethora of information through their isotope geochemistry, TREE geochemistry, and mineral inclusions, the interpretation of these data is not always straightforward and similar datasets have resulted in vastly different conclusions (Harrison et al., 2008; Rollinson, 2008; Kemp et al., 2010; Rasmussen et al., 2010, 2011; Carley et al., 2022). In addition, a comparison to modern TREE in zircon may not be adequate since conditions (e.g., higher heat flux from the mantle, reduced mantle viscosity) and hence tectonic processes were likely different compared to today. Previous work proposed that Archean TTGs may be possible analogues to settings in which the Hadean Green Sandstone Bed (GSB) zircons formed (Carley et al., 2022). To test this, we will compare and contrast Archean detrital zircons to >3.8 Ga zircons from the GSB. During this comparative analysis, we will refer to the zircons from the Green Sandstone Bed as "GSB" zircons and those from the Moodies and Fig Tree Groups as "BGGT" zircons. While the zircons of the GSB are theoretically part of the BGGT, they show a significantly different zircon age distribution and Cr-spinel geochemistry, and hence a fundamentally different source terrane to that of the BGGT (see section 5.3).

The Isotope and TREE geochemistry of the GSB are discussed in detail by Drabon et al., (2021,2022). The 4.2 to 3.3 Ga detrital zircon suite of the GSB shows a notable transition in its geochemistry at 3.8 Ga (Drabon et al., 2022). Zircons older than 3.8 Ga have been interpreted to reflect long-lived, mantle-derived protocrust that experienced no juvenile additions based on the array of decreasing ϵ_{HfT} with time and mantle-like TREE signatures (Drabon et al., 2021, 2022).

The geochemical and isotopic composition of BGGT detrital zircons show significant differences to those >3.8 Ga of the GSB. The starkest difference is seen in the Hf isotope record (Fig. 8A). BGGT zircons do not show evidence for intracrustal reworking without juvenile additions; instead, each episode of felsic crust formation shows a mix of juvenile additions together with remelting of older crust, with the mean of each age cluster being close to CHUR. The TREE geochemistry of BGGT zircons also shows some notable differences, with none of the BGGT zircons showing the same distribution of Sc/Yb and U/Nb data as the pre-3.8 Ga GSB zircons (Fig. 8C; 2D Kolmogorov-Smirnov test; p<8x10⁻⁷). The most favorable comparison is for Group 2 of the 3.29 Ga cluster and the 3.55 Ga zircon cluster, which partially overlap with the pre-3.8 Ga GSB zircons (Fig. 8C). However, the 3.29 Ga and the 3.55 Ga BGGT zircons have

higher U values compared to pre-3.8 Ga GSB zircons. This may hint at remelting of some pre-existing hydrated crust for the BGGT zircons, melting at different depth, and/or a shift in mantle composition. The 3.46 Ga age cluster, which has been suggested to be an analogue for Hadean crust formation in the Jack Hills (Laurent et al., 2022), shows fundamental differences to the >3.8 Ga GSB zircons when Sc and Nb are considered. Lastly, GSB and BGGT zircons show a similar range in $\delta^{18}{\rm O}$ values but differ in their clustering (Fig. 8B). BGGT zircons show distinct clustering while pre-3.8 Ga GSB zircons instead show a wide range of values from mantle to supercrustal values for their 400 Ma history without any distinct clustering. This may be related to a wide range of sources rather than a limited number of sources as is the case for the detrital zircons of the Fig Tree and Moodies Groups.

In summary, Barberton felsic igneous rocks and co-magmatic volcanic rocks are not good analogues for the majority of Hadean zircon of the GSB. We argue that the majority of pre-3.8 Ga zircons of the GSB formed in vastly different tectono-magmatic environments to those of volcanic and plutonic igneous rocks of the BGGT due to their differences in crustal residence time and in volume of hydrous melting.

5.3. Comparison of the evolution of the source terrane(s) to the GSB and BGGT and implications for the formation of Archean proto-continental crust

One unresolved question in early Earth relates to the timing and process of continent formation. The detrital zircons from the BGGT and GSB combined span $\sim \! 900$ million years, between 4.15 and 3.22 Ga, providing two complementary geochemical records of early crust generation.

The BGGT and GSB detritus tapped largely different sources of two neighboring terranes. Many of the detrital zircon and spinel grains of the GSB appear to have been derived from outside the BGGT or from units currently unrecognized within the Barberton area (Byerly et al., 2018; Drabon et al., 2021, 2022). In terms of felsic igneous sources, most zircon age clusters seen in the GSB (3.31 Ga, 3.38 Ga, 4.1 Ga) are not seen in 112 detrital zircon sandstone samples collected throughout the greenstone belt (Fig. 9A) (Drabon et al., 2021). In terms of mafic igneous sources, the dominant Cr-spinel population from the GSB does not overlap in its geochemistry with those of associated komatiitic flow sequences of the Mendon Formation (Byerly et al., 2018; Drabon et al., 2021). Many of the zircons and chromites are well rounded, suggesting that they have been transported for long distances and/or experienced efficient reworking while being transported from their respective sources, possibly by aeolian processes (Lowe et al., 2021). On the other hand, there is some evidence for a connection between the two terranes. Firstly, proposed aeolian transport of relatively coarse GSB detritus, much coarser (\sim 150 µm; Lowe et al., 2021) than typical wind-blown loess (<20 µm) that can be blown for great distances, would be limited to at least connected terranes. Secondly, there is some overlap in ages: the 3.65 Ga age cluster in the GSB is represented by rare detrital zircons of the same age in Moodies and Fig Tree sediments and both have a similar geochemical signature (Fig. 9); the major 3.38 Ga event in the GSB source terrane may be represented in the Barberton area by dykes intruding the Theespruit Pluton dated at 3383 $\pm\,11$ Ma and 3388 \pm 38 Ma (Moyen et al., 2019). Thirdly, negative ϵ_{HfT} values of two Theespruit tuffs may represent some reworking of pre-3.8 Ga protocrust. Lastly, the BGGT and GSB zircon suites show similar, albeit not concurrent, changes through time in their zircon geochemistry (Fig. 9). These similar stages of crustal evolution within the two terranes may reflect the diachronous evolution of tectonic processes across two connected terranes. As a more recent example, rifting that opened the Rocas Verdes back-arc basin during the Jurassic and earliest Cretaceous and associated rift volcanism commenced diachronously over tens of millions of years and hundreds of kilometers (Malkowski et al., 2016). However, the difference in timing of the onset of extension and shortening of tens of millions of years between the GSB and the BGGT

suggests that the two terranes must have been quite far apart, possibly hundreds of kilometers.

In summary, the use of detrital zircons allows us to study the geochemical evolution of a much larger number of felsic igneous events than are preserved in the Barberton region, recorded by detrital zircons derived from crust that is now lost or deeply buried. Combining both the BGGT and GSB zircon data provides a prime example of the geochemical evolution of Archean continents and, while speculative until whole rocks that sourced the GSB are found, reveals our preferred model of the buildup of Archean proto-continental crust includes at least four stages (Figs. 9 and 10):

Stage I (Long-lived protocrust; Fig. 10A): The formation of a dominantly mafic crustal nucleus was initiated by extraction from the mantle between 4.4 and 4.2 Ga (Drabon et al., 2022). This crust experienced continuous intracrustal reworking with no, or only very limited, evidence for juvenile felsic additions and hydrous melting (Fig. 9). The continuous mantle signature as suggested by zircon trace elements indicates that arc-accretion was not a major process. Importantly, the zircon geochemical signatures are significantly different from those of < 3.8 Ga zircons from the GSB and BGGT, implying that crustal processes, conditions, and/or source materials were vastly different.

Stage II (crustal growth; Fig. 10B): The onset of crustal growth and magmatic thickening though frequent juvenile felsic additions, crustal reworking, and the onset of fluid-assisted melting, possibly at greater depths. This started at \sim 3.8 Ga in the GSB and at least since 3.65 Ga in the BGGT source terranes. Zircons <3.8 Ga in the GSB show abundant similarities to those of the BGGT, including common CHUR-like ϵ_{HfT} and hydrous melting TREE signatures (Drabon et al., 2022; Fig. 9B, D, E).

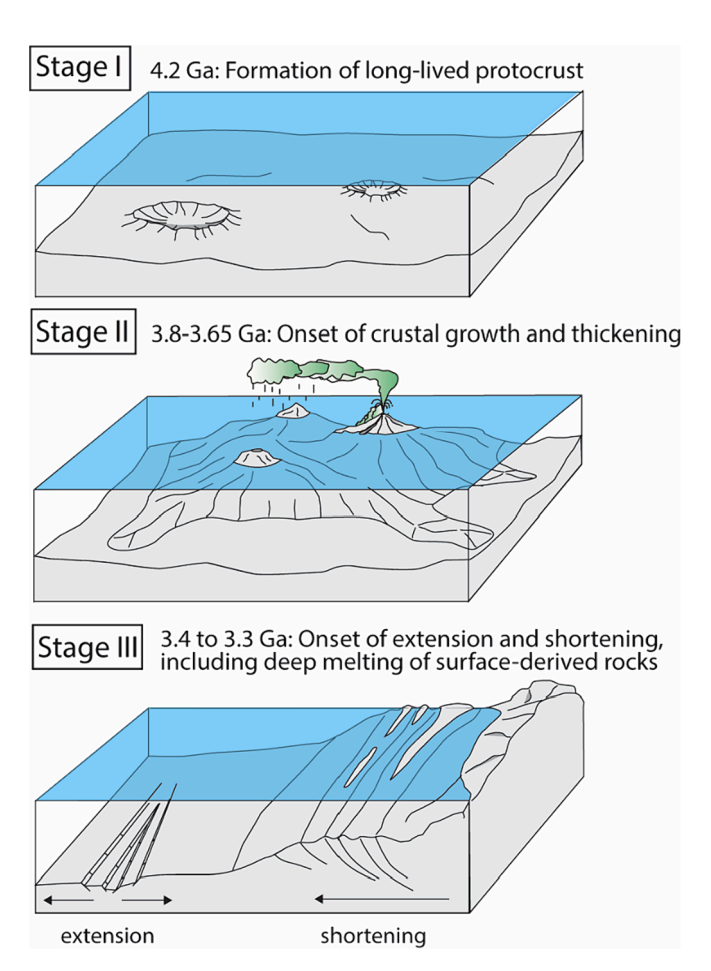


Fig. 10. Block diagrams representing the proposed crustal evolution. [Stage I] Formation of long-lived crust, [Stage II] formation of an oceanic plateau, and [Stage III] onset of extension and shortening.

Isotopic evidence for the Hadean protocrust is almost entirely lost during this time period (Fig. 9B), either because it was small in extent or because it was not involved in subsequent melting. In either case, our data provide no evidence for a substantial Hadean continental basement below the BGGT. Our results are consistent with formation of an oceanic plateau for the BGGT, as suggested for the evolution of the Onverwacht Group due to the lack of evidence for tectonic deformation (e.g., Byerly et al., 2019; Moyen et al., 2019), but horizontal tectonics cannot be excluded based on the zircon geochemistry alone.

Stage III (extension and shortening; Fig. 10C):

Stage IIIa: The abrupt influx of mantle material in an extensional setting (3.38 Ga in the GSB and 3.29 Ga in the BGGT). In both regions, this can be traced by a sharp drop in Sc/Yb and elevated Nb values (Fig. 9D and E). The occurrence of the lowest Eu/Eu* and Sc/Yb values in both sequences (Fig. 9F) may relate to melting and fractionation within the plagioclase stability field, hence melting at relatively shallow depth of a mafic precursor derived from the mantle. In the BGGT, geological relations support mantle-plume induced extension (Lowe, 1999; Trower and Lowe, 2016). In the GSB, low δ^{18} O values and high Ti values are similar to plume/extensional settings (Stelten et al., 2014; Zhu et al., 2021). The similar evolution of the two source terranes at this time suggests a connectivity of the two terranes at least since Stage III.

Stage IIIb: This episode is dominated by crustal reworking and characterized by zircon signatures more akin to modern subduction zones (3.31 Ga in the GSB and 3.28 Ga in the BGGT). This includes an increase in hydrous melting (highest Sc/Yb), associated with an apparent shift to deeper melting and/or more oxidizing conditions (increase in Eu/Eu*, Dy/Yb) (Fig. 9E, F). In the BGGT, this is the first time when TREE and O isotopes reflect deep melting of surface-derived rocks. It is quite remarkable that this is the first time in almost 900 million years of crustal evolution in the area. Overall, this time period may mark the onset of crustal amalgamation and thickening. While controversy exists as to what the exact tectonic setting was during that time, stratigraphic and structural data suggest at least some subhorizontal shortening (Drabon and Lowe, 2022; Heubeck et al., 2023). The close association between mantle plume/extension and lateral accretion may reflect a cause-and-effect mechanism. For example, some form of hot proto-subduction may have been triggered by gravitational instability due to the initiation of extension (Tang et al., 2020) or plume activity (Gerya et al., 2015). Other, non-uniformitarian triggers may have been subduction triggered by meteorite impacts such as suggested for the S6 and S8 impact events at ~3.3 Ga recorded in the Barberton area (O'Neill et al., 2020). More work will be necessary to deduce a possible causeand-effect relationship.

Stage IV: Craton stabilization: Although not part of this study, previous work identified a final episode of generation of a large, buoyant continental block, today represented by the Kaapvaal Craton. This episode is characterized by gradual crustal stabilization and thickening through intrusion of large potassic granitic batholiths, intracrustal melting, several phases of regional metamorphism, and late-stage deformation between 3.216 Ga and ~3.1 Ga (Westraat et al., 2005; Belcher and Kisters, 2006; Schoene and Bowring, 2010; Byerly et al., 2019). This episode occurred long after sedimentation and deformation in the BGGT had ceased (Byerly et al., 2019).

As detailed above, the formation of the Archean continental crust in the Barberton area can be seen as evolving through several stages from static to more dynamic: from Stage I during which felsic crust formed in long-lived protocrust, to Stage II significant crustal growth and magmatic thickening perhaps in a mafic plateau, and Stage III horizontal mobility expressed by extension and shortening, the latter of which caused tectonic amalgamation and thickening. While the zircon geochemical signatures during Stage III would be consistent with modern plate tectonics, it is unclear whether plate tectonics were even rheologically feasible during the early Earth due to the hotter mantle (Davies, 2009; Herzberg et al., 2010; Ganne and Feng, 2017; Korenaga, 2018). While these conditions may have hindered the development of

senso stricto modern-style plate tectonics, they would have still allowed for some compression and shortening, based on numerical modeling (Sizova et al., 2010; Wang et al., 2018; Tang et al., 2020). In either case, continent formation in the Barberton region was a multi-step process that may have included some form of horizontal tectonics in the latter half of its formation.

6. Conclusion

The Barberton Greenstone Belt reveals a rich geochemical record of crustal evolution and geodynamics covering almost a billion years of felsic crust generation, only about half of which is recorded in the wholerock record. Detrital and tuffaceous zircons thus provide a more complete picture of the crustal evolution in the broader Barberton region, revealing several insights:

- (1) The broad trends in the elementally partitioned geochemistry of zircons from known sources matches that of related whole-rocks and the local geology, showing that zircon can record crustal conditions and source compositions of melts in which they formed in many instances when multiple geochemical proxies are combined. However, it is important to note that zircons may be crystallizing from residual melts produced by differentiation of the parental melt and may hence vary in detail from the bulk composition of its source (Laurent et al., 2022).
- (2) In every age cluster (3.65, 3.55, 3.45, 3.28, and <3.29 Ga) for Barberton detrital zircons (excluding GSB zircons) at least some of the zircon compositions indicate evidence for hydrous melting, indicating that the different types of processes that melted hydrated rock were active throughout the time of greenstone belt evolution.
- (3) There were two major episodes of mantle extraction in the BGGT at ~3.65–3.80 Ga and, previously unrecognized, at 3.29 Ga. Both are followed by episodes of dominated by crustal reworking, but only the latter event was immediately followed by a major tectonic episode of orogenesis that initiated the generation of topography and siliciclastic debris, and culminated in the onset of deep recycling of surface-derived materials at 3.23 Ga.
- (4) Barberton TTGs are not a good analogue for Hadean crust formation as indicated by a comparison to the oldest zircons in the Green Sandstone Bed. The Hadean zircons from the GSB are vastly different to the Barberton TTG zircons in their ε_{HfT}, δ¹⁸O and TREE signatures, suggesting that they formed by different processes, under different conditions, and/or from different source materials.
- (5) The geochemical and tectonic evolution of the broader Barberton region (incl. detrital zircons of the Moodies, Fig Tree groups, and the GSB) occurred in several stages, with zircon signatures for zircons younger than <3.4 Ga being most similar to that of modern plate tectonics. While it is unclear if this last stage represents plate or squishy-lid tectonics, it does suggest that Archean continent formation and the onset of modern-style plate tectonics was a multi-step process spanning hundreds of millions of years in the Barberton region.

Data availability

Data are available through Mendeley Data at https://data.mendeley.com/datasets/zmj566r6m4/2.

CRediT authorship contribution statement

Nadja Drabon: Writing – original draft, Visualization, Validation, Supervision, Resources, Project administration, Methodology, Investigation, Funding acquisition, Formal analysis, Data curation, Conceptualization. Heather M. Kirkpatrick: Writing – review & editing,

Visualization. Gary R. Byerly: Writing – review & editing. Joseph L. Wooden: Writing – review & editing, Validation, Investigation, Formal analysis.

Declaration of competing interest

The authors declare that they have no known competing financial interests or personal relationships that could have appeared to influence the work reported in this paper.

Acknowledgements

We thank Sappi and the Mpumalanga Tourism and Parks Agency for access to lands. Funding for travel expenses and analytical costs were kindly provided by the Stanford School of Earth, Energy, and Environmental Sciences at Stanford University and the Earth and Planetary Sciences Department at Harvard University, ND was financially supported through the Liebermann Fellowship from Stanford University and by the Earth and Planetary Sciences Department at Harvard University. At the USGS Menlo Park, Ruth Dawn's and David Damby's help during the acquisition of CL images was greatly appreciated. The staff of the Arizona LaserChron Center, especially Mark Pecha, Kurt Sundell, and George Gehrels, at the University of Arizona and Christine Jilly-Rehak at the SHRIMP-RG laboratory at Stanford University were very helpful during detrital zircon analyses. We also thank Michael Wiedenbeck and Frédéric Couffignal who provided key analtical support in the Potsdam SIMS lab. We greatly appreciated discussions with Christoph Heubeck, Jean-François Moyen, and Donald Lowe about the general geological evolution of the Barberton Greenstone Belt. Finally, we thank Gary Stevens and Simon Wilde for constructive and insightful reviews of the manuscript.

Appendix A. Supplementary material

Supplementary material includes a detailed description of the methods for trace and rare earth element, Lu-Hf isotope, and O isotope data acquisition. Additional figures include a compilation of previously dated detrital zircon used in the study (Fig. S1), a U vs U/Nb plot (Fig. S2), a principal component analysis of BGGT data only (Fig. S3) and one that includes different age clusters of the GSB (Fig. S4), and a ϵ_{HfT} vs time plot including possible source rocks (Fig. S5). Supplementary material to this article can be found online at https://doi.org/10.1016/j.gca.2024.03.014.

References

- Agangi, A., Hofmann, A., Elburg, M.A., 2018. A review of Palaeoarchaean felsic volcanism in the eastern Kaapvaal craton: linking plutonic and volcanic records. Geosci. Front. 9, 667–688.
- Armstrong, R.A., Compston, W., de Wit, M.J., Williams, I.S., 1990. The stratigraphy of the 3.5-3.2 Ga Barberton Greenstone Belt revisited: a single zircon ion microprobe study. Earth Planet. Sci. Lett. 101, 90–106.
- Arndt, N., 2023. How did the continental crust form: No basalt, no water, no granite. Precambr. Res. 397, 107196.
- Baier, J., Audétat, A., Keppler, H., 2008. The origin of the negative niobium tantalum anomaly in subduction zone magmas. Earth Planet. Sci. Lett. 267, 290–300.
- Bédard, J.H., 2018. Stagnant lids and mantle overturns: Implications for Archaean tectonics, magmagenesis, crustal growth, mantle evolution, and the start of plate tectonics. Geosci. Front. 9, 19–49.
- Bédard, J.H., Harris, L.B., Thurston, P.C., 2013. The hunting of the snArc. Precambr. Res. 229, 20–48.
- Belcher, R.W., Kisters, A.F.M., 2006. Syntectonic emplacement and deformation of the Heerenveen batholith: Conjectures on the structural setting of the 3.1 Ga granite magmatism in the Barberton granite-greenstone terrain, South Africa. In: Reimold, W.U., Gibson, R.L. (Eds.), Processes on the Early Earth. Geological Society of America, pp. 211–231.
- Bell, E.A., Boehnke, P., Hopkins-Wielicki, M.D., Harrison, T.M., 2015. Distinguishing primary and secondary inclusion assemblages in Jack Hills zircons. Lithos 234–235, 15–26.
- Byerly, G.R., Kröner, A., Lowe, D.R., Todt, W., Walsh, M.M., 1996. Prolonged magmatism and time constraints for sediment deposition in the early Archean Barberton

- greenstone belt: evidence from the Upper Onverwacht and Fig Tree groups. Precambr. Res. 78, 125–138.
- Byerly, B.L., Lowe, D.R., Drabon, N., Coble, M.A., Burns, D.H., Byerly, G.R., 2018. Hadean zircon from a 3.3 Ga sandstone, Barberton greenstone belt, South Africa. Geology 46, 967–970.
- Byerly, G.R., Lowe, D.R., Heubeck, C., 2019. Geologic Evolution of the Barberton Greenstone Belt—A Unique Record of Crustal Development, Surface Processes, and Early Life 3.55–3.20 Ga. In: Van Kranendonk, M.J., Bennett, V.C., Hoffmann, J.E. (Eds.), Earth's Oldest Rocks. Elsevier, pp. 569–613.
- Carley, T.L., Bell, E.A., Miller, C.F., Claiborne, L.L., Hunt, A., Kirkpatrick, H.M., Harrison, T.M., 2022. Zircon-modeled melts shed light on the formation of Earth's crust from the Hadean to the Archean. Geology 50, 1028–1032.
- Cavosie, A.J., Valley, J.W., Wilde, S.A., 2005. Magmatic δ18O in 4400–3900 Ma detrital zircons: A record of the alteration and recycling of crust in the Early Archean. Earth Planet. Sci. Lett. 235, 663–681.
- Cavosie, A.J., Kita, N.T., Valley, J.W., 2009. Primitive oxygen-isotope ratio recorded in magmatic zircon from the Mid-Atlantic Ridge. Am. Mineral. 94, 926–934.
- Cawood, P.A., Chowdhury, P., Mulder, J., Hawkesworth, C.J., Capitanio, F.A., Gunawardana, P.M., Nebel, O., 2022. Secular evolution of continents and the earth system. Rev. Geophys. 60, e2022RG000789.
- Claiborne, L.L., Miller, C.F., Wooden, J.L., 2010. Trace element composition of igneous zircon: A thermal and compositional record of the accumulation and evolution of a large silicic batholith, Spirit Mountain, Nevada. Contrib. Mineral. Petrol. 160, 511–531.
- Clemens, J.D., Yearron, L.M., Stevens, G., 2006. Barberton (South Africa) TTG magmas: Geochemical and experimental constraints on source-rock petrology, pressure of formation and tectonic setting. Precambr. Res. 151, 53–78.
- Clemens-Knott, D., Surpless, K.D., Barth, A.P., Wooden, J.L., 2021. Leveraging detrital zircon geochemistry to study deep arc processes: REE-rich magmas mobilized by Jurassic rifting of the Sierra Nevada arc. Results in Geochemistry 4, 100010.
- Coble, M.A., Vazquez, J.A., Barth, A.P., Wooden, J., Burns, D., Kylander-Clark, A., Jackson, S., Vennari, C.E., 2018. Trace Element Characterisation of MAD-559 Zircon Reference Material for Ion Microprobe Analysis. Geostand. Geoanal. Res. 42, 481-497
- Davies, G.F., 2009. Effect of plate bending on the Urey ratio and the thermal evolution of the mantle. Earth Planet. Sci. Lett. 287, 513–518.
- de Ronde, C.E.J., Kamo, S.L., 2000. An Archaean arc-arc collisional event. Journal of African Earth Sciences (1994), 30, 219–248.
- de Ronde, C.E.J., de Wit, M.J., 1994. Tectonic history of the Barberton greenstone belt, South Africa: 490 million years of Archean crustal evolution. Tectonics 13, 983–1005.
- de Ronde, C.E.J., Kamo, S., Davis, D.W., de Wit, M.J., Spooner, E.T.C., 1991. Field, geochemical and U-Pb isotopic constraints from hypabyssal felsic intrusions within the Barberton greenstone belt, South Africa: Implications for tectonics and the timing of gold mineralization. Precambr. Res. 49, 261–280.
- De Wit, M.J., 1998. On Archean granites, greenstones, cratons, and tectonics: does the evidence demand a verdict? Precambr. Res. 91, 181–226.
- de Wit, M.J., Armstrong, R., Hart, R.J., Wilson, A.H., 1987a. Felsic igneous rocks within the 3.3- to 3.5-Ga Barberton Greenstone Belt: High crustal level equivalents of the surrounding Tonalite-Trondhjemite Terrain, emplaced during thrusting. Tectonics 6, 529–549
- de Wit, M.J., Hart, R.A., Hart, R.J., 1987b. The Jamestown Ophiolite Complex, Barberton mountain belt: a section through 3.5 Ga oceanic crust. J. Afr. Earth Sc. 6, 681–730.
- de Wit, M.J., Furnes, H., Robins, B., 2011. Geology and tectonostratigraphy of the Onverwacht Suite, Barberton Greenstone Belt, South Africa. Precambr. Res. 186, 1, 27
- de Wit, M.J., 1991. Archaean greenstone belt tectonism and basin development. J. Afr. Earth Sci. (1994). 13, 45–63.
- Decker, N.B., Byerly, G.R., Thompson Stiegler, M., Lowe, D.R., Stefurak, E., 2015. High resolution tephra and U/Pb chronology of the 3.33–3.26 Ga Mendon Formation, Barberton Greenstone Belt, South Africa. Precambr. Res. 261, 54–74.
- Diergaardt, B.N., 2013. Rhyolitic volcanism in the Onverwacht Group, Barberton Greenstone Belt (M.Sc. Thesis). Stellenbosch University, Stellenbosch.
- Drabon, N., Lowe, D.R., Byerly, G.R., Harrington, J.A., 2017. Detrital zircon geochronology of sandstones of the 3.6-3.2 Ga Barberton greenstone belt: No evidence for older continental crust. Geology 45, 803–806.
- Drabon, N., Galić, A., Mason, P.R.D., Lowe, D.R., 2019a. Provenance and tectonic implications of the 3.28–3.23 Ga Fig Tree Group, central Barberton greenstone belt, South Africa. Precambr. Res. 325, 1–19.
- Drabon, N., Heubeck, C.E., Lowe, D.R., 2019b. Evolution of an Archean fan delta and its implications for the initiation of uplift and deformation in the Barberton Greenstone Belt, South Africa. J. Sediment. Res. 89.
- Drabon, N., Byerly, B.L., Byerly, G.R., Wooden, J.L., Keller, C.B., Lowe, D.R., 2021. Heterogeneous Hadean crust with ambient mantle affinity recorded in detrital zircons of the Green Sandstone Bed, South Africa. PNAS 118, e2004370118.
- Drabon, N., Byerly, B.L., Byerly, G.R., Wooden, J.L., Wiedenbeck, M., Valley, J.W., Kitajima, K., Bauer, A.M., Lowe, D.R., 2022. Destabilization of long-lived hadean protocrust and the onset of pervasive hydrous melting at 3.8 Ga. AGU Adv. 3, e2021AV000520.
- Drabon, N., Lowe, D.R., 2022. Progressive accretion recorded in sedimentary rocks of the 3.28-3.23 Ga Fig Tree Group, Barberton Greenstone Belt. Bull. Geol. Soc. Am. 134, 1258–1276.
- Dziggel, A., Kisters, A.F.M., 2019. Tectonometamorphic controls on archaean gold mineralization in the barberton greenstone Belt, South Africa. In: Van Kranendonk, M.J., Bennett, V.C., Hoffmann, J.E. (Eds.), Earth's Oldest Rocks. Elsevier, pp. 655–674.

- Eriksson, K.A., 1980. Transitional sedimentation styles in the Moodies and Fig Tree Groups, Barberton Mountain Land, South Africa: Evidence favouring an Archean continental margin. Precambr. Res. 12, 141–160.
- Ernst, W.G., Liu, J., 1998. Experimental phase-equilibrium study of Al- and Ti-contents of calcic amphibole in MORB-A semiquantitative thermobarometer. Am. Mineral. 83, 952–969.
- Furnes, H., de Wit, M.J., Robins, B., Sandstå, N.R., 2011. Volcanic evolution of the upper Onverwacht Suite, Barberton Greenstone Belt, South Africa. Precambr. Res. 186, 28–50.
- Furnes, H., Robins, B., De Wit, M.J., 2012. Geochemistry and petrology pf lavas in the upper Onverwacht Suite, Barberton Mountain Land, South Africa. S. Afr. J. Geol. 115, 171–210
- Furnes, H., de Wit, M., Robins, B., 2013. A review of new interpretations of the tectonostratigraphy, geochemistry and evolution of the Onverwacht Suite, Barberton Greenstone Belt, South Africa. Gondw. Res.
- Gaetani, G.A., Asimow, P.D., Stolper, E.M., 2008. A model for rutile saturation in silicate melts with applications to eclogite partial melting in subduction zones and mantle plumes. Earth Planet. Sci. Lett. 272, 720–729.
- Ganne, J., Feng, X., 2017. Primary magmas and mantle temperatures through time. Geochem. Geophys. Geosyst. 18, 872–888.
- Gehrels, G., Pecha, M., 2014. Detrital zircon U-Pb geochronology and Hf isotope geochemistry of Paleozoic and Triassic passive margin strata of western North America. Geosphere 10, 49–65.
- Gerya, T.V., Stern, R.J., Baes, M., Sobolev, S.V., Whattam, S.A., 2015. Plate tectonics on the Earth triggered by plume-induced subduction initiation. Nature 527, 221–225.
- Goodwin, A.M., 1996. Distribution and tectonic setting of Precambrian crust. In: Goodwin, A. (Ed.), Principles of precambrian geology. Academic Press, New York, pp. 1–50.
- Green, T.H., 1982. Anatexis of mafic crust and high pressure crystallization of andesite. Am. Soc. Mech. Eng. (paper) 465–487.
- Grimes, C.B., John, B.E., Kelemen, P.B., Mazdab, F.K., Wooden, J.L., Cheadle, M.J., Hanghøj, K., Schwartz, J.J., 2007. Trace element chemistry of zircons from oceanic crust: A method for distinguishing detrital zircon provenance. Geology 35, 643–646.
- Grimes, C.B., Wooden, J.L., Cheadle, M.J., John, B.E., 2015. "Fingerprinting" tectonomagmatic provenance using trace elements in igneous zircon. Contrib. Miner. Petrol. 170, 1–26.
- Harrison, T.M., Schmitt, A.K., McCulloch, M.T., Lovera, O.M., 2008. Early (≥ 4.5 Ga) formation of terrestrial crust: Lu-Hf, δ18O, and Ti thermometry results for Hadean zircons. Earth Planet. Sci. Lett. 268, 476–486.
- Harrison, T.M., Bell, E.A., Boehnke, P., 2017. Hadean Zircon Petrochronology. Rev. Mineral. Geochem. 83, 329–363.
- Herzberg, C., Condie, K., Korenaga, J., 2010. Thermal history of the Earth and its petrological expression. Earth Planet. Sci. Lett. 292, 79–88.
- Heubeck, C., Lowe, D.R., 1994. Late syndepositional deformation and detachment tectonics in the Barberton Greenstone Belt. South Africa. Tectonics 13, 1514–1536.
- Heubeck, C., Drabon, N., Byerly, G., Leisgang, I., Linnemann, U., Lowe, D., Mertz-Kraus, R., Gonzalez-Pinzon, A., Thomsen, T.B., Zeh, A., Rojas-Agramonte, Y., Kröner, A., 2022. Detrital zircon provenance of the Archean Moodies Group, Barberton Greenstone Belt, South Africa and Eswatini. Am. J. Sci. 322, 65–107.
- Heubeck, C., Lowe, D.R., 1999. Sedimentary petrography and provenance of the Archean Moodies Group, Barberton Greenstone Belt. In: Lowe, D.R., Byerly, G.R. (Eds.), Geologic evolution of the barberton greenstone belt. Geological Society of America, South Africa, pp. 259–286.
- Heubeck, C., Thomsen, T.B., Heredia, B.D., Zeh, A., Balling, P., 2023. The Malolotsha Klippe: Large-Scale Subhorizontal Tectonics Along the Southern Margin of the Archean Barberton Greenstone Belt, Eswatini. Tectonics 42, e2022TC007359.
- Hoffmann, E.J., Kröner, A., 2019. Early Archean Crustal Evolution in Southern Africa—An Updated Record of the Ancient Gneiss Complex of Swaziland. In: Van Kranendonk, M.J., Bennett, V.C., Hoffmann, J.E. (Eds.), Earth's Oldest Rocks. Elsevier, pp. 553–567.
- Hopkins, M., Harrison, T.M., Manning, C.E., 2008. Low heat flow inferred from >4 Gyr zircons suggests Hadean plate boundary interactions. Nature 456, 493–496.
- Hoskin, P.W.O., Black, L.P., 2002. Metamorphic zircon formation by solid-state recrystallization of protolith igneous zircon. J. Metam. Geol. 18, 423–439.
- Hoskin, P.W.O., Schaltegger, U., 2003. The composition of zircon and igneous and metamorphic petrogenesis. Rev. Mineral. Geochem. 53, 27–62.
- Ibanez-Mejia, M., Gehrels, G.E., Ruiz, J., Vervoort, J.D., Eddy, M.E., Li, C., 2014. Small-volume baddeleyite (ZrO2) U-Pb geochronology and Lu-Hf isotope geochemistry by LA-ICP-MS. Techniques and applications. Chem. Geol. 384, 149–167.
- Jackson, M.P.A., Eriksson, K.A., Harris, C.W., 1987. Early Archean foredeep sedimentation related to crustal shortening: a reinterpretation of the Barberton Sequence, Southern Africa. Tectonophysics 136, 197–221.
- Jagoutz, O., Schmidt, M.W., Enggist, A., Burg, J.P., Hamid, D., Hussain, S., 2013. TTGtype plutonic rocks formed in a modern arc batholith by hydrous fractionation in the lower arc crust. Contrib. Miner. Petrol. 166, 1099–1118.
- John, T., Klemd, R., Klemme, S., Pfänder, J.A., Hoffmann, J.E., Gao, J., 2011. Nb-Ta fractionation by partial melting at the titanite-rutile transition. Contrib. Miner. Petrol. 161, 35–45.
- Johnson, T.E., Brown, M., Gardiner, N.J., Kirkland, C.L., Smithies, R.H., 2017. Earth's first stable continents did not form by subduction. Nature 543, 239–242.
- Kamo, S.L., Davis, D.W., 1994. Reassessment of Archean crustal development in the Barberton Mountain Land, South Africa, based on U-Pb dating. Tectonics 13, 167–192.
- Kemp, A.I.S., Wilde, S.A., Hawkesworth, C.J., Coath, C.D., Nemchin, A., Pidgeon, R.T., Vervoort, J.D., DuFrane, S.A., 2010. Hadean crustal evolution revisited: New

- constraints from Pb-Hf isotope systematics of the Jack Hills zircons. Earth Planet. Sci. Lett. 296, 45–56.
- Kisters, A.F.M., Belcher, R.W., Poujol, M., Dziggel, A., 2010. Continental growth and convergence-related arc plutonism in the Mesoarchaean: Evidence from the Barberton granitoid-greenstone terrain, South Africa. Precambr. Res. 178, 15–26.
- Kleinhanns, I.C., Kramers, J.D., Kamber, B.S., 2003. Importance of water for Archaean granitoid petrology: A comparative study of TTG and potassic granitoids from Barberton Mountain Land, South Africa. Contrib. Miner. Petrol. 145, 377–389.
- Korenaga, J., 2018. Crustal evolution and mantle dynamics through Earth history. Philos. Trans. R. Soc. A Math. Phys. Eng. Sci. 376, 20170408.
- Kröner, A., Byerly, G.R., Lowe, D.R., 1991. Chronology of early Archaean granitegreenstone evolution in the Barberton Mountain Land, South Africa, based on precise dating by single zircon evaporation. Earth Planet. Sci. Lett. 103, 41–54.
- Kröner, A., Hegner, E., Wendt, J.I., Byerly, G.R., 1996. The oldest part of the Barberton granitoid-greenstone terrain, South Africa: evidence for crust formation between 3.5 and 3.7 Ga. Precambr. Res. 78, 105–124.
- Kröner, A., Anhaeusser, C.R., Hoffmann, J.E., Wong, J., Geng, H., Hegner, E., Xie, H., Yang, J., Liu, D., 2016. Chronology of the oldest supracrustal sequences in the Palaeoarchaean Barberton Greenstone Belt, South Africa and Swaziland. Precambr. Res. 279, 123–143.
- Kröner, A., Todt, W., 1988. Single zircon dating constraining the maximum age of the Barberton greenstone belt, southern Africa. J. Geophys. Res. Solid Earth 93, 15329–15337.
- Lamb, S.H., 1984. Structures on the eastern margin of the Archaean Barberton greenstone belt, northwest Swaziland. In: Kröner, A., Greiling, R. (Eds.), Precambrian Tectonics Illustrated. Schweizerbart, Stuttgart, Germany, pp. 19–39.
- Lamb, S., Paris, I., 1988. Post-Onverwacht Group stratigraphy in the SE part of the Archaean Barberton greenstone belt. Journal of African Earth Sciences (1994). 7, 285–306
- Laurent, O., Björnsen, J., Wotzlaw, J.F., Bretscher, S., Pimenta Silva, M., Moyen, J.-F., Ulmer, P., Bachmann, O., 2020. Earth's earliest granitoids are crystal-rich magma reservoirs tapped by silicic eruptions. Nat. Geosci. 13, 163–169.
- Laurent, O., Moyen, J.-F., Wotzlaw, J.F., Björnsen, J., Bachmann, O., 2022. Early Earth zircons formed in residual granitic melts produced by tonalite differentiation. Geology 50, 437–441.
- Laurie, A., Stevens, G., 2012. Water-present eclogite melting to produce Earth's early felsic crust. Chem. Geol. 314–317, 83–95.
- Li, L., Xiong, X.L., Liu, X.C., 2017. Nb/Ta Fractionation by Amphibole in Hydrous Basaltic Systems: Implications for Arc Magma Evolution and Continental Crust Formation. J. Petrol. 58, 3–28.
- Lowe, D.R., 1994. Accretionary history of the Archean Barberton Greenstone Belt (3.55-3.22 Ga), southern Africa. Geology 22, 1099–1102.
- Lowe, D.R., Drabon, N., Byerly, G.R., Byerly, B.L., 2021. Windblown Hadean zircons derived by erosion of impact-generated 3.3 Ga uplifts, Barberton Greenstone Belt, South Africa. Precambr. Res. 356, 106111.
- Lowe, D.R., Nocita, B.W., 1999. Foreland basin sedimentation in the Mapepe Formation, southern-facies Fig Tree Group. In: Lowe, D.R., Byerly, G.R. (Eds.), Geologic Evolution of the Barberton Greenstone Belt. Geological Society of America, South Africa, pp. 233–258.
- Lowe, D.R., Byerly, G.R., Heubeck, C., 2012. Geologic map of the Barberton Greenstone Belt. Geological Society of America." Map and Chart Series 103.
- Lowe, D. R., 1999. Geologic evolution of the Barberton Greenstone Belt and vicinity. In: Lowe, Donald R., Byerly, G.R. (Eds.), Geologic Evolution of the Barberton Greenstone Belt, South Africa. Geological Society of America, pp. 287–312.
- Lowenstern, J.B., Clynne, M.A., Bullen, T.D., 1997. Comagmatic A-type granophyre and rhyolite from the Alid volcanic center, Eritrea, northeast Africa. J. Petrol. 38, 1707–1721.
- Lowenstern, J.B., Charlier, B.L.A., Clynne, M.A., Wooden, J.L., 2006. Extreme U-Th disequilibrium in rift-related basalts, rhyolites and granophyric granite and the timescale of rhyolite generation, intrusion and crystallization at Alid volcanic center, Eritrea. J. Petrol. 47, 2105–2122.
- Malkowski, M.A., Grove, M., Graham, S.A., 2016. Unzipping the Patagonian Andes—Long-lived influence of rifting history on foreland basin evolution. Lithosphere 8, 23–28.
- $Martin,\,H.,\,1986.\,Effect\,\,of\,\,steeper\,\,Archean\,\,geothermal\,\,gradient\,\,on\,\,geochemistry\,\,of\,\,subduction-zone\,\,magmas.\,\,Geology\,\,14,\,\,753-756.$
- Matsumura, R., 2014. The Petrogenesis of the Nelshoogte Pluton: The Youngest and Most Compositionally Variable TTG Pluton in the Barberton Granite-greenstone Terrain (M.Sc.). Stellenbosch University, Stellenbosch
- McDowell, S.M., Miller, C.F., Mundil, R., Ferguson, C.A., Wooden, J.L., 2014. Zircon evidence for a \sim 200 k.y. supereruption-related thermal flare-up in the Miocene southern Black Mountains, western Arizona, USA. Contrib. Miner. Petrol. 168, 1031.
- Moyen, J.-F., 2011. The composite Archaean grey gneisses: Petrological significance, and evidence for a non-unique tectonic setting for Archaean crustal growth. Lithos 123, 21–36
- Moyen, J.-F., Stevens, G., Kisters, A.F.M., Belcher, R.W., 2007. Chapter 5.6 TTG Plutons of the Barberton Granitoid-Greenstone Terrain, South Africa. Developments in Precambrian Geology. 15, 607–667.
- Moyen, J.-F., Laurent, O., 2018. Archaean tectonic systems: A view from igneous rocks. Lithos 302–303, 99–125.
- Moyen, J.-F., Martin, H., 2012. Forty years of TTG research. Lithos.
- Moyen, J.-F., Stevens, G., Kisters, A., 2006. Record of mid-Archaean subduction from metamorphism in the Barberton terrain, South Africa. Nature 442, 559–562.
- Moyen, J.-F., Stevens, G., Kisters, A.F.M., Belcher, R.W., Lemirre, B., 2019. TTG Plutons of the Barberton Granitoid-Greenstone Terrain, South Africa. In: Van

- Kranendonk, M.J., Bennett, V.C., Hoffmann, J.E. (Eds.), Earth's Oldest Rocks. Elsevier, pp. 615–653.
- Nagel, T.J., Hoffmann, J.E., Münker, C., 2012. Generation of Eoarchean tonalitetrondhjemite-granodiorite series from thickened mafic arc crust. Geology 40, 375–378.
- O'Neill, C., Marchi, S., Bottke, W., Fu, R., 2020. The role of impacts on Archaean tectonics. Geology 48, 174–178.
- Pearce, J.A., 1982. Trace element characteristics of lavas from destructive plate boundaries. In: Thorpe, R.S. (Ed.), Andesites: Orogenic Andesites and Related Rocks. John Wiley and Sons, New York, pp. 525–548.
- Pedersen, T., Heeremans, M., Van Der Beek, P., 1998. Models of crustal anatexis in volcanic rifts: Applications to southern Finland and the Oslo Graben, southeast Norway. Geophys. J. Int. 132, 239–255.
- Petersson, A., Kemp, A.I.S., Gray, C.M., Whitehouse, M.J., 2020. Formation of early Archean Granite-Greenstone Terranes from a globally chondritic mantle: Insights from igneous rocks of the Pilbara Craton, Western Australia. Chem. Geol. 551, 119757.
- Rasmussen, B., Fletcher, I.R., Muhling, J.R., Wilde, S.A., 2010. In situ U-Th-Pb geochronology of monazite and xenotime from the Jack Hills belt: Implications for the age of deposition and metamorphism of Hadean zircons. Precambr. Res. 180, 26-46
- Rasmussen, B., Fletcher, I.R., Muhling, J.R., Gregory, C.J., Wilde, S.A., 2011.
 Metamorphic replacement of mineral inclusions in detrital zircon from Jack Hills,
 Australia: Implications for the Hadean Earth. Geology 39, 1143–1146.
- Reimer, T.O., Condie, K.C., Schneider, G., Georgi, A., 1985. Petrography and geochemistry of granitoid and metamorphite pebbles from the early Archaean Moodies Group, Barberton Mountainland/south Africa. Precambr. Res. 29, 383–404.
- Robb, L.J., Barton, J.M., Kable, E.J.D., Wallace, R.C., 1986. Geology, geochemistry and isotopic characteristics of the Archaean Kaap Valley pluton, Barberton Mountain Land, South Africa. Precambr. Res. 31, 1–36.
- Roerdink, D.L., Mason, P.R.D., Whitehouse, M.J., Brouwer, F.M., 2016. Reworking of atmospheric sulfur in a Paleoarchean hydrothermal system at Londozi, Barberton Greenstone Belt, Swaziland. Precambr. Res. 280, 195–204.
- Rollinson, H., 2008. Ophiolitic trondhjemites: A possible analogue for Hadean felsic "crust". Terra Nova 20, 364–369.
- Ryerson, F.J., Watson, E.B., 1987. Rutile saturation in magmas: implications for TiNbTa depletion in island-arc basalts. Earth Planet. Sci. Lett. 86, 225-239.
- Sanchez-Garrido, C.J.M.G., Stevens, G., Armstrong, R.A., Moyen, J.-F., Martin, H., Doucelance, R., 2011. Diversity in earth's early felsic crust: Paleoarchean peraluminous granites of the Barberton Greenstone Belt. Geology 39, 963–966.
- Schmitz, M., Heubeck, C., 2021. Constraints on deformation mechanisms of the Barberton Greenstone Belt from regional stratigraphic and structural data of the synorogenic Moodies Group. Precambr. Res. 362, 106177.
- Schoene, B., Bowring, S.A., 2010. Rates and mechanisms of Mesoarchean magmatic arc construction, eastern Kaapvaal craton, Swaziland. Bull. Geol. Soc. Am. 122, 408–429.
- Schoene, B., de Wit, M.J., Bowring, S.A., 2008. Mesoarchean assembly and stabilization of the eastern Kaapvaal craton: A structural-thermochronological perspective. Tectonics 27.
- Sizova, E., Gerya, T., Brown, M., Perchuk, L.L., 2010. Subduction styles in the Precambrian: Insight from numerical experiments. Lithos 116, 209–229.
- Stelten, M.E., Cooper, K.M., Vazquez, J.A., Calvert, A.T., Glessner, J.J.G., 2014. Mechanisms and timescales of generating eruptible rhyolitic magmas at Yellowstone Caldera from Zircon and sanidine geochronology and geochemistry. J. Petrol. 56, 1607–1642.
- Stepanov, A.S., Hermann, J., 2013. Fractionation of Nb and Ta by biotite and phengite: Implications for the "missing Nb paradox". Geology 41, 303–306.
- Stern, R.J., 2005. Evidence from ophiolites, blueschists, and ultrahigh-pressure metamorphic terranes that the modern episode of subduction tectonics began in Neoproterozoic time. Geology 33, 557–560.
- Stevens, G., Moyen, J.F., 2007. Chapter 5.7 Metamorphism in the Barberton Granite Greenstone Terrain: A Record of Paleoarchean Accretion. Developments in Precambrian Geology. 15, 669–698.
- Stoll, E., Drabon, N., Lowe, D.R., 2021. Provenance and paleogeography of Archean Fig Tree siliciclastic rocks in the East-Central Barberton Greenstone Belt, South Africa. Precambr. Res. 354, 106041.
- Stutenbecker, L., Heubeck, C., Zeh, A., 2019. The lomati delta complex: A prograding tidal delta in the archean moodies group, barberton greenstone belt. S. Afr. J. Geol. 122, 17–38.
- Tang, M., Lee, C.T.A., Chen, K., Erdman, M., Costin, G., Jiang, H., 2019. Nb/Ta systematics in arc magma differentiation and the role of arclogites in continent formation. Nature Communications 2019 10:1. 10, 1–8.

- Tang, M., Ji, W.Q., Chu, X., Wu, A., Chen, C., 2021. Reconstructing crustal thickness evolution from europium anomalies in detrital zircons. Geology 49, 76–80.
- Tang, C.A., Webb, A.A.G., Moore, W.B., Wang, Y.Y., Ma, T.H., Chen, T.T., 2020. Breaking Earth's shell into a global plate network. Nat. Commun. 11, 3621.
- Tice, M.M., Bostick, B.C., Lowe, D.R., 2004. Thermal history of the 3.5-3.2 Ga Onverwacht and Fig Tree Groups, Barberton greenstone belt, South Africa, inferred by Raman microspectroscopy of carbonaceous material. Geology 32, 37–40.
- Trail, D., Watson, E.B., Tailby, N., 2010. New experimental constraints for Hadean zircon source melts from Ce and Eu anomalies in zircon. American Geophysical Union, Fall Meeting.
- Trail, D., Watson, E.B., Tailby, N.D., 2012. Ce and Eu anomalies in zircon as proxies for the oxidation state of magmas. Geochim. Cosmochim. Acta 97, 70–87.
- Trower, E.J., Lowe, D.R., 2016. Sedimentology of the ~3.3 Ga upper Mendon Formation, Barberton Greenstone Belt, South Africa. Precambr. Res. 281, 473–494.
- Tusch, J., Hoffmann, J.E., Hasenstab, E., Fischer-Gödde, M., Marien, C.S., Wilson, A.H., Münker, C., 2022. Long-term preservation of Hadean protocrust in Earth's mantle. PNAS 119, e2120241119.
- Valley, J.W., 2003. Oxygen isotopes in zircon. Rev. Mineral. Geochem. 53, 343–385.
 Valley, J.W., Kinny, P.D., Schulze, D.J., Spicuzza, M.J., 1998. Zircon megacrysts from kimberlite: Oxygen isotope variability among mantle melts. Contrib. Miner. Petrol.
- Valley, J.W., Lackey, J.S., Cavosie, A.J., Clechenko, C.C., Spicuzza, M.J., Basei, M.A.S., Bindeman, I.N., Ferreira, V.P., Sial, A.N., King, E.M., Peck, W.H., Sinha, A.K., Wei, C. S., 2005. 4.4 billion years of crustal maturation. Contrib. Miner. Petrol. 150, 151, 150.
- Van Kranendonk, M.J., 2021. Gliding and overthrust nappe tectonics of the Barberton Greenstone Belt revisited: A review of deformation styles and processes. S. Afr. J. Geol. 124, 181–210.
- Van Kranendonk, M.J., Kröner, A., Hoffman, J.E., Nagel, T., Anhaeusser, C.R., 2014. Just another drip: Re-analysis of a proposed Mesoarchean suture from the Barberton mountain land, South Africa. Precambr. Res. 254, 19–35.
- Van Kranendonk, M.J., Hugh Smithies, R., Griffin, W.L., Huston, D.L., Hickman, A.H., Champion, D.C., Anhaeusser, C.R., Pirajno, F., 2015. Making it thick: A volcanic plateau origin of Palaeoarchean continental lithosphere of the Pilbara and Kaapvaal cratons. Geochem. Soc. Spec. Publ. 389, 83–111.
- Van Kranendonk, M.J., 2011. Cool greenstone drips and the role of partial convective overturn in Barberton greenstone belt evolution. Journal of African Earth Sciences (1994), 60, 346–352.
- Wang, X., Tang, M., Moyen, J.-F., Wang, D., Kröner, A., Hawkesworth, C., Xia, X., Xie, H., Anhaeusser, C., Hofmann, A., Li, J., Li, L., 2022b. The onset of deep recycling of supracrustal materials at the Paleo-Mesoarchean boundary. National Science. Review 9. nwab136.
- Wang, H., van Hunen, J., Pearson, D.G., 2018. Making Archean cratonic roots by lateral compression: A two-stage thickening and stabilization model. Tectonophysics 746, 562–571.
- Wang, H., Yang, J.H., Zhu, Y.S., Huang, C., Xu, L., Wu, S.T., Liu, Y., 2022a. Archean crustal growth and reworking revealed by combined U-Pb-Hf-O isotope and trace element data of detrital zircons from ancient and modern river sediments of the eastern Kaapvaal Craton. Geochim. Cosmochim. Acta 320, 79–104.
- Westraat, J.D., Kisters, A.F.M., Poujol, M., Stevens, G., 2005. Transcurrent shearing, granite sheeting and the incremental construction of the tabular 3.1 Ga Mpuluzi batholith, Barberton granite-greenstone terrane, South Africa. J. Geol. Soc. London 162, 373–388
- Wiemer, D., Schrank, C.E., Murphy, D.T., Wenham, L., Allen, C.M., 2018. Earth's oldest stable crust in the Pilbara Craton formed by cyclic gravitational overturns. Nat. Geosci. 11, 357–361.
- Xie, X., Byerly, G.R., Ferrell Jr., R.E., 1997. IIb trioctahedral chlorite from the Barberton greenstone belt: crystal structure and rock composition constraints with implications to geothermometry. Contrib. Miner. Petrol. 126, 275–291.
- Xiong, X., Keppler, H., Audétat, A., Gudfinnsson, G., Sun, W., Song, M., Xiao, W., Yuan, L., 2009. Experimental constraints on rutile saturation during partial melting of metabasalt at the amphibolite to eclogite transition, with applications to TTG genesis. Am. Mineral. 94, 1175–1186.
- Zeh, A., Gerdes, A., Heubeck, C., 2013. U-Pb and Hf isotope data of detrital zircons from the Barberton greenstone belt: Constraints on provenance and Archaean Crustal evolution. J. Geol. Soc. London 170, 215–223.
- Zhu, J., Zhang, Z., Tan, S., Jin, Z., Santosh, M., 2021. Intracontinental rift-related magmatism in the eastern Emeishan Large Igneous Province traced by zircon oxygen isotopes. Lithos 406–407.